3. SYSTEMS ANALYSIS

Ronald L. Miller

Contents

3. SYSTEMS ANALYSIS

3.1. INTRODUCTION

The SPPS Systems Activity integrates physics, engineering, and costing models to identify potentially attractive stellarator power-plant design points for further detailed analysis. Additionally, trade and parametric studies establish key sensitivities of the stellarator approach.

The objective of the Systems Activity is to study and determine systematically plant operating parameters through economic analysis and optimization of the power station, with an emphasis placed on the performance of the fusion power core (FPC). The FPC includes the plasma chamber, first wall, divertor, blanket, shield, coils, and associated structure. A reference design point is chosen to meet overall design goals of the SPPS, such as minimal cost of electricity (COE) and high mass power density (MPD, defined as the ratio of net-electric-power output to the mass of the FPC). Trade-off and sensitivity studies are performed to establish and characterize the design window for optimal magnetic fusion power plants. Results and constraints from more detailed modeling and engineering design efforts are fed back and integrated into the systems model. The systems code is, therefore, used as a tool in the iterative conceptual engineering-design process. The Systems Analysis approach used for the SPPS is consistent with the recent ARIES [1] and PULSAR [2] tokamak conceptual designs, although the SPPS level of effort is smaller than that of the tokamak studies.

The ARIES Systems Code (ASC), described in detail in Ref. [1], was modified for use in the SPPS; the modified version is denoted "ASC*" in this report. Typically, the projected cost of electricity (COE, mill/kWeh) is used as a object function to be minimized. Certain descriptive material is recapitulated here from the corresponding section of Ref. [1]. Some explanations relating to the cost models and assumptions that may be unfamiliar to the stellarator community are retained here for their tutorial value. New material, particularly that reporting code modifications from ASC to ASC*, appropriate to present stellarator applications, is also included.

Section 3.2 summarizes the plasma, FPC, power plant, and costing models that are used in the ASC*. The reference SPPS design point, based on the Modular Helias-like Heliac (MHH), is reported in Sec. 3.3. Results [3] dating from an early phase of the SPPS for a Compact Torsatron (CT) have not been brought up to date using the final ASC* costing groundrules, but those results are thought to remain generally comparable. The results of parametric and sensitivity studies about the SPPS/MHH reference design point are discussed in Sec. 3.4. Conclusions drawn from this work are summarized in Sec. 3.5. An Appendix to this report contains a more comprehensive listing of physics, engineering, and economic parameters and results produced by the ASC* for the SPPS/MHH.

3.2. MODELS AND METHODS

The SPPS systems studies activity integrates physics, engineering, and costing models to identify potentially attractive deuterium-tritium magnetic-fusion power-plant design points for further detailed analysis. Additionally, trade and parametric studies establish key sensitivities of the stellarator approach and help sort through the several competing variants. Where appropriate, assumptions, models, and materials choices in common with the recent ARIES [1] and PULSAR [2] tokamak power plant studies are employed to facilitate meaningful comparisons.

3.2.1. Plasma Engineering

The ASC* model for plasma engineering is a steady-state, point-plasma (zero-dimensional) model that is adjusted to simulate two-dimensional profile effects. Features of this model are discussed in this subsection. The SPPS/MHH deuterium-tritium (DT) plasma would operate at (or slightly below) ignition, heated primarily by the fusion-product alpha particles.

3.2.1.1. Preliminaries

Plasma Geometry. The SPPS/MHH plasma geometry incorporates a non-planar-axis, quasi-toroidal plasma column with a periodic, but variable cross section [4]. Representative elevation views at selected toroidal positions along a field period are illustrated in Fig. 3.2-1. Anticipating the baseline SPPS/MHH baseline design point, the MHH0103 configuration has been scaled to a major toroidal radius, $R_T = 13.95$ m, denoted by the "+" symbol. The crescent-shaped plasma cross section is at the largest major toroidal radius at the position, $\phi = 0°$, corresponding to the MHH corner. The last closed plasma flux surface is indicated by the dashed line. The outermost solid contour denotes the

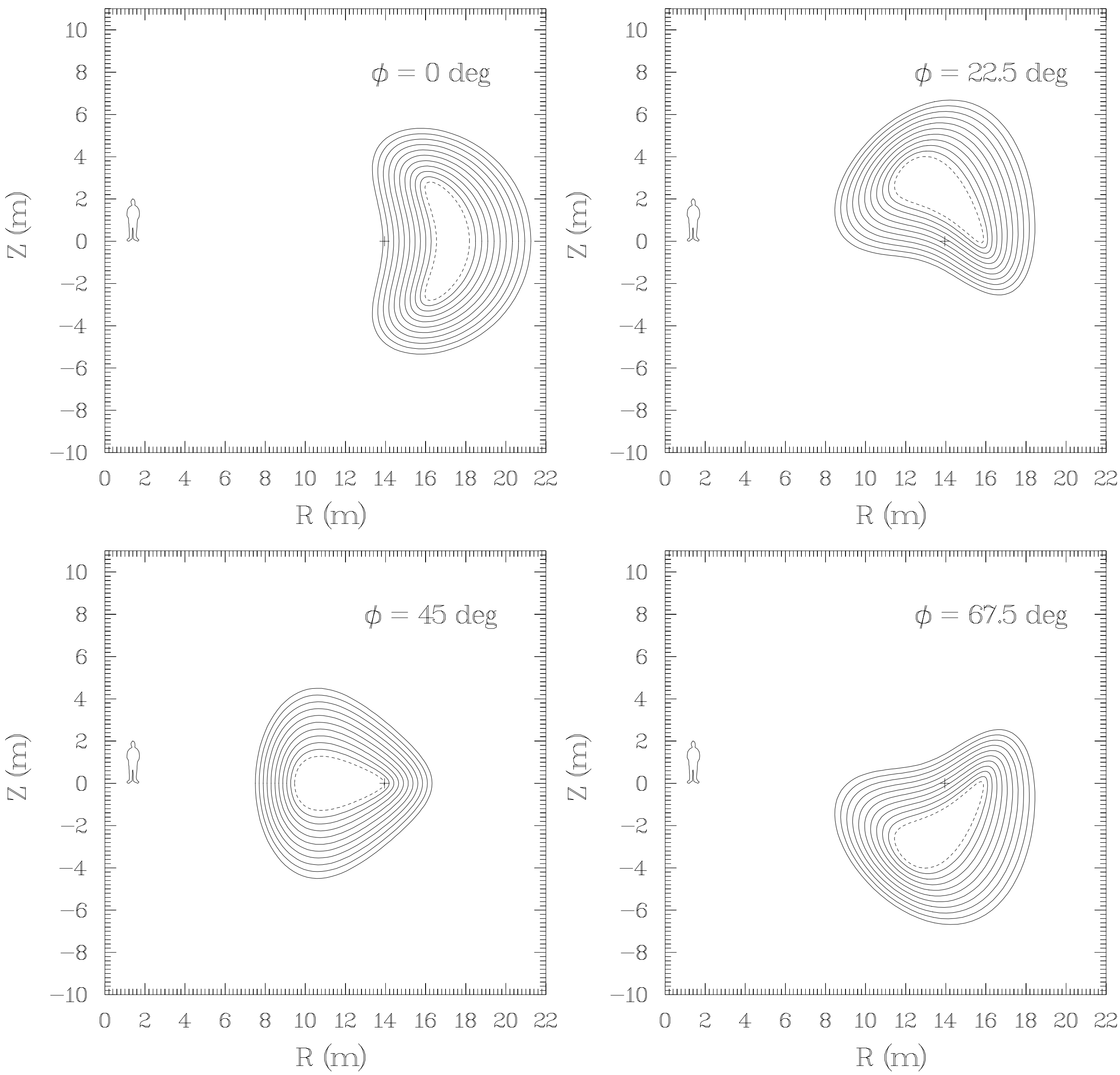

Figure 3.2-1. Schematic elevation views of the SPPS/MHH plasma outer (last closed) flux surface (dashed line at $\rho = 0$), modular-coil centroid (outer solid line at $\rho = 1$), and intermediate phantom surfaces ($\delta\rho = 0.1$) for the four-field-period MHH0103 case [4] scaled to a major toroidal radius, $R_T = 13.95$ m at several toroidal locations denoted by the angle, ϕ. The view at $\phi = 90°$ returns to that at $\phi = 0°$ to define the periodicity of the configuration. See Fig. 3.2-2 for representative three-dimensional views of the plasma surface.

centroid of the modular coil as projected into the $\phi = constant$ plane. The actual coil dimension is determined by the required on-axis magnetic-field strength and a nominal coil current density, as discussed below. Intermediate conformal contours are indicated by the remaining solid lines; the innermost solid line need not indicate the position of the first wall. These contours are suggestive of the nested blanket and shield geometries that must be accomodated, together with the divertor, in the SPPS/MHH configuration. The available standoff distance between the plasma surface and the coil centroid shrinks as the major radius is reduced, thus inhibiting reductions in fusion power core size and access to the higher-power density operating regime.

As a simplification for purposes of the ASC*, the effective toroidal plasma geometry is described by the equivalent major toroidal radius, R_T, and minor plasma radius, a_p (*i.e.*, half width of the minor plasma diameter at the mid-plane), and vertical half height, b, defining the elongation, $\kappa_\times = b/a_p$. The plasma aspect ratio is $A \equiv R_T/a_p = 1/\epsilon$. The average plasma cross-sectional area is given by

$$A_p \;=\; \pi a_p^2 \kappa_\times \;\equiv\; \pi r_p^2 \,, \tag{3.2-1}$$

where r_p is the circularized (average) plasma radius. The corresponding effective major toroidal radius of the centroid of the plasma cross section is R_T for the MHH. The plasma aspect ratio is $A \equiv R_T/a_p = 1/\epsilon$ in the usual tokamak parlance, or $A^\star \equiv R_T/r_p$ for the MHH. The plasma volume is conveniently given by $V_p \equiv 2\pi R_T A_p$. Then,

$$V_p \;=\; 2\pi^2 \, R_T \, a_p^2 \, \kappa_\times \,. \tag{3.2-2}$$

The actual geometrical quantities derived from separate numerical calculations [4] are calibrated by the simplified ASC* approximations. Results are summarized in Table 3.2-I. While the primary goal of the approximation in matching the plasma volume has been met, it is not possible to recover simultaneously the large plasma surface area of the MHH plasma. Thus, the first-wall neutron wall load is overestimated by the approximate model (see Sec. 5.3.2).

Thermal Plasma Constituency. The same temperature profile, $T_i(r)$, is assumed to describe all background ions. Therefore, the total ion density, n_i, the electron density, n_e (assuming charge neutrality), and the effective ionic charge, Z_{eff}, are obtained by summing over the ion species. Calculation of the average Z and Z^2 of impurity species assumes coronal equilibrium.

Table 3.2-I.
SPPS/MHH Plasma Geometry[a]

Plasma major 'toroidal' radius, R_T (m)	13.95
Plasma half-width, a_p (m)	1.155
Plasma aspect ratio (*cf.*, tokamak), $A \equiv R_T/a_p$	12.08
Plasma elongation, $\kappa_\times$	2.0
Circularized (average) plasma radius, r_p (m)	1.633
Plasma aspect ratio, $A^\star \equiv R_T/r_p$	8.54
Average plasma cross-sectional area, A_p (m^2)	8.38[b]
Plasma volume, V_p (m^3)	734.7
First-wall surface area[c], A_{FW} (m^2)	1,171

[a] *cf.*, Ref. [4].

[b] Compare with MHH0103 value of 8.39 m^2.

[c] Compare with MHH0103 plasma-surface area of 1,233 m^2.

The plasma ion and electron densities are denoted by n_i and n_e, respectively. Local charge neutrality requires that

$$n_e(r) = \sum_j n_j(r) Z_j \; , \tag{3.2-3}$$

where the summation is over all ion species (*i.e.*, fuel, fusion products, and impurities). The effective plasma charge is defined as

$$Z_{eff} \;=\; \frac{\sum\limits_j n_j Z_j^2}{\sum\limits_j n_j Z_j} \; , \tag{3.2-4}$$

and the effective square of the plasma charge is defined as

$$Z_{eff}^2 \;=\; \frac{\sum\limits_j n_j Z_j^3}{n_e Z_{eff}} \; . \tag{3.2-5}$$

The Maxwellian plasma ion population consists of deuterium (D) and tritium (T) as the primary fuel species; fusion-product α-particles (^{4}He), proton (p), and helium-3 (^{3}He); and assumed impurities (1% O). The concentration of each ion species (other than oxygen) $f_j \equiv n_j/n_i$ is calculated with the continuity equations described below. For the baseline SPPS/MHH design point, $f_D \simeq 0.470$, $f_T \simeq 0.471$, and $f_{^3He} \simeq 0.047$ to yield $Z_{eff} \simeq 1.59$.

Radial Plasma Profiles. The following general forms are assumed for the density profile for all species, the temperature profile for all thermal species, and the toroidal current-density profile:

$$n(x) = (n_o - n_s)(1-x)^{\alpha_n} + n_s \ , \tag{3.2-6}$$

$$T(x) = T_o(1-x)^{\alpha_T} \ , \tag{3.2-7}$$

$$j_\phi(x) = j_o(1-x)^{\alpha_J} \ ; \tag{3.2-8}$$

where $x \equiv (r/r_p)^2$ and the α_n, α_T, and α_J are fitting constants that are adjusted to fit reference radial profiles. With no net plasma current in the stellarator, Eq. (3.2-8) is of interest only for tokamak applications. A non-zero edge-plasma density, n_s, is included to lower the peak heat flux and plasma temperature at the divertor plate. Approximating the plasma as a circular cylinder with concentric flux surfaces, profile form factors are calculated for all terms.

The volume-averaged current density, plasma density, temperature, and density-weighted volume-averaged temperature are defined, respectively, as follows:

$$j_\phi \equiv \frac{I_\phi}{A_p} \ , \tag{3.2-9}$$

$$n \equiv \frac{2\pi}{A_p}\int_0^{r_p} n(r)\, rdr \ , \tag{3.2-10}$$

$$\bar{T} \equiv \frac{2\pi}{A_p}\int_0^{r_p} T(r)\, rdr \ , \tag{3.2-11}$$

$$T \equiv \frac{2\pi}{n\,A_p}\int_0^{r_p} T(r)\, n(r)\, rdr \ , \tag{3.2-12}$$

where I_ϕ is the toroidal plasma current, of no interest for stellarator applications. These integrations yield

$$\frac{n}{n_o} = \frac{1}{1+\alpha_n(1-n_s/n)} \ , \tag{3.2-13}$$

$$\frac{\bar{T}}{T_o} = \frac{1}{1+\alpha_T}\,, \tag{3.2-14}$$

$$\frac{T}{T_o} = \frac{1+\alpha_n\{1-\alpha_T n_s/[n(1+\alpha_T)]\}}{1+\alpha_n+\alpha_T}\,. \tag{3.2-15}$$

Equilibrium and stability considerations dictate the pressure profile, $p(r)[\propto n(r)T(r)]$, consistent with the magnetohydrodynamic (MHD) properties of the configuration. The simplified one-dimensional density and temperature profiles used herein are required to reproduce the peak-to-average values of the pressure and density that are obtained from the more detailed calculations of equilibrium and stability, as discussed in Sec. 2.

Representative radial plasma profiles for the SPPS/MHH are illustrated in Fig. 3.2-2, and profile inputs to the ASC* are summarized in Table 3.2-II. The improved perfor-

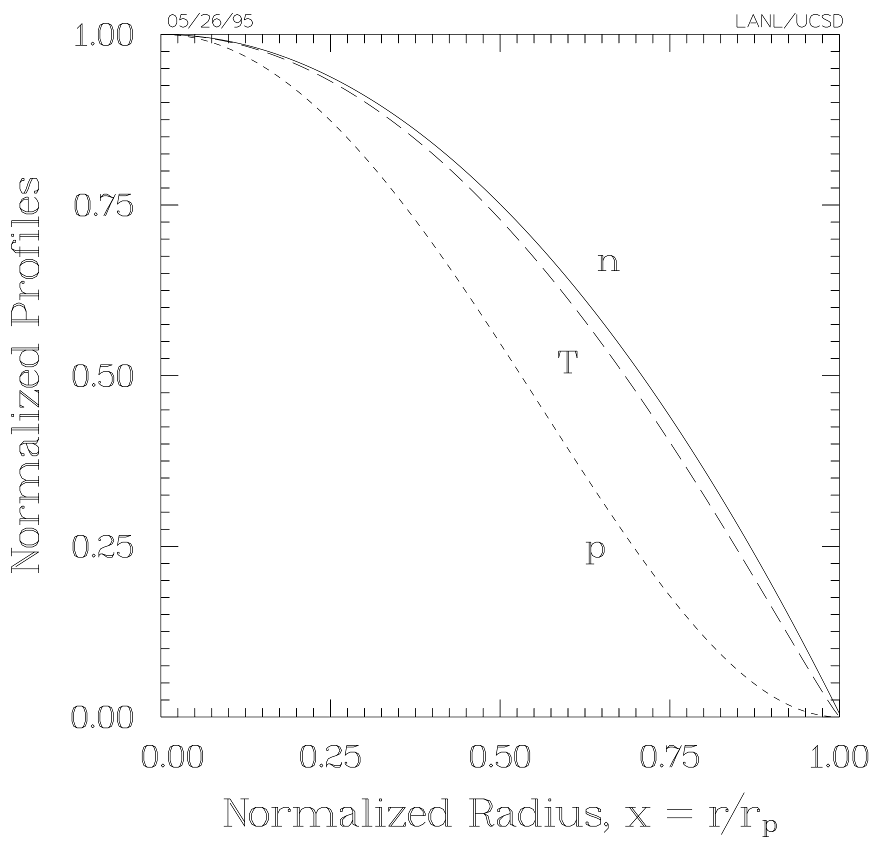

Figure 3.2-2. Density, $n(x)$, temperature, $T(x)$, and pressure, $p(x)$, radial profiles, where $x \equiv r/r_p$, used in the ASC* for the MHH. See Table 3.2-II for more profile information.

Table 3.2-II.
Profile Inputs[a] to the ASC and ASC⋆ and Other Profile Information

Parameter	ARIES-I	ARIES-II/IV	SPPS/MHH
Peak-to-average pressure, $p_0/p(=n_0T_0/nT)$	2.47	$\boxed{2.97}$	3.09
Peak-to-average density, n_0/n	1.30	$\boxed{1.12}$	1.99
Peak-to-average temperature,[b] T_0/T	1.90	2.65	1.55
Peak-to-average temperature,[c] $T_0/\bar{T}$	2.10	2.84	2.10
Separatrix-to-average density, n_s/n	$\boxed{0.70}$	$\boxed{0.45}$	$\boxed{0.01}$
Density profile exponent, α_n	$\boxed{1.00}$	0.22	$\boxed{1.00}$
Temperature profile exponent, α_T	$\boxed{1.10}$	1.84	$\boxed{1.10}$
Pressure profile exponent, α_p	2.10	1.97	2.10
Current-density profile exponent, α_J	3.48	2.55	NA
Profile form factors[d], g_k:			
– Fusion reactions:			
g_{DT}	1.081	1.369	1.924
g_{DDn}	1.327	1.718	1.941
g_{DDp}	1.327	1.655	1.915
g_{D^3He}	—	5.876	3.364
– Bremsstrahlung radiation:			
g_{BR}	1.050	0.941	1.396

(a) Input values are boxed.

(b) The density-weighted, volume-averaged temperature.

(c) The volume-averaged temperature.

(d) As described in Sec. 3.2.1.2.

mance of the ARIES-II/IV [1] gaseous divertor permited a lower density pedestal than was used for ARIES-I [5] to allow penetration of lower-hybrid (LH) current drive into the edge plasma region. In the absence of detailed information regarding the implications and consequences of stellarator edge performance, the edge-density pedestal for the SPPS/MHH case was suppressed. This issue should be revisited in any future studies with a view toward developing a self-consistent picture of the core plasma and the scrape-off layer (SOL) in interaction with the divertor as the impurity-control system. The issue of the possible advantage or need of a radiating mantle to spread power over the entire first-wall surface area, sparing the divertor surfaces was not explored during the present study.

Plasma Beta. The magnetic field produced by external coils provides the confining field in stellarators for the plasma pressure, p. The on-axis toroidal magnetic-field strength is $B(R_T) \equiv B_o$, the toroidal beta is $\beta \equiv 2\mu_o B_o^2$, where $\mu_o \equiv 4\pi \times 10^{-7}$ H/m is the permeability of free space. The beta value of the reference SPPS/MHH configuration is taken to be 5% (see Sec. 2).

The fractional beta supported by athermal fusion products, $f_{\beta H}$, is calculated by integrating over their slowing-down distributions. The relationship between the thermal plasma pressure and the total beta is given by

$$\beta(1 - f_{\beta H} - f_{\beta B}) = \frac{2\mu_o k_B(n_i T_i + n_e T_e)}{B_{\phi o}^2}\,, \tag{3.2-16}$$

where $f_{\beta B}$ is the fractional beta introduced by any neutral beams (not used for the SPPS/MHH, such that $f_{\beta B} = 0$). For the SPPS/MHH, the value of $f_{\beta H} \simeq 0.06$.

The inputs to the ASC* equilibrium model are derived from detailed equilibrium and stability calculations (Sec. 2). It would be desirable to have a representative scaling relation for β as a function of plasma aspect ratio, A, radial profile parameters, *etc.*, in order to exercise the optimization capabilities of the ASC*. Such a relation was not available for the SPPS, thus limiting the study to the characterization of the MHH to a representative, but not globally optimized, case.

3.2.1.2. Particle and Power Balance

The plasma particle- and power-balance module used in the ASC* is based on the zero-dimensional (0-D), steady-state MakNTAU [1, 6, 7] code. The model used in this module is summarized in this subsection with a detailed description given in Ref. [6]. Profile effects are included in the model through radial averages over the profiles given by Eqs. (3.2-6)-(3.2-8) above.

Profile Averaging. A volume-averaged power density is denoted by p_k and, assuming toroidal symmetry, is defined as

$$p_k \equiv \frac{2\pi}{A_p} \int_0^{r_p} p_k(j(r), n(r), T(r)) r dr \, ; \tag{3.2-17}$$

where the subscript k denotes a power generation or loss process (*e.g.*, fusion, radiation, or ohmic-heating). The volume-averaged power density can be written as a product of a profile-form factor, g_k, that contains the profile information and a "mean" power density that is evaluated at the average plasma parameters, *i.e.*,

$$p_k = g_k \, p_k(j_\phi, n, T) \, . \tag{3.2-18}$$

The profile-form factor is then defined as

$$g_k \equiv \frac{2\pi}{p_k(j_\phi, n, T) \, A_p} \int_0^{r_p} p_k \, (j(r), n(r), T(r)) \; r dr \, . \tag{3.2-19}$$

The total power is then given by

$$P_k \equiv V_p p_k \, . \tag{3.2-20}$$

Several fusion reactions, dominated by $T(d,n)^4He$ at $T \simeq 10$ keV, would occur in the MHH plasma and are summarized on Table 3.2-III. Using the definition of the profile form factor, the average fusion power density for the k^{th} reaction is given by

$$p_{Fk} = g_k \, n_l n_m \, \langle \sigma v \rangle_k \, Q_k \, , \tag{3.2-21}$$

where $\langle \sigma v \rangle_k$ is the Maxwellian-averaged fusion reactivity that is evaluated at the density-weighted, volume-averaged ion temperature, and g_k is the fusion-power profile-form factor. The volume-averaged plasma ion density, n_i, has several fuel-ion constituents denoted by separate subscripts (*e.g.*, l, m, *etc.*), which participate in the various possible fusion reactions. The values of $\langle \sigma v \rangle_k$ are obtained using R-matrix fits [8]. The ion-temperature dependence of $\langle \sigma v \rangle_k$ is illustrated in Fig. 3.2-3.

The results of the profile averaging of the fusion reactivity are used in the other plasma engineering modules. For example, the average-fusion-reaction-rate density that is used in the particle-balance model is given by

$$R_{lm} = g_k \, n_l n_m \, \langle \sigma v \rangle_k \, . \tag{3.2-22}$$

Table 3.2-III.
Dominant Fusion Reactions

k	Reaction	Q_k (MeV/fusion)
DT	$D + T \rightarrow n + {}^4He$	17.586
DD	$D + D \rightarrow p + T$	4.032
	$D + D \rightarrow n + {}^3He$	3.267
D ^{3}He	$D + {}^3He \rightarrow p + {}^4He$	18.341

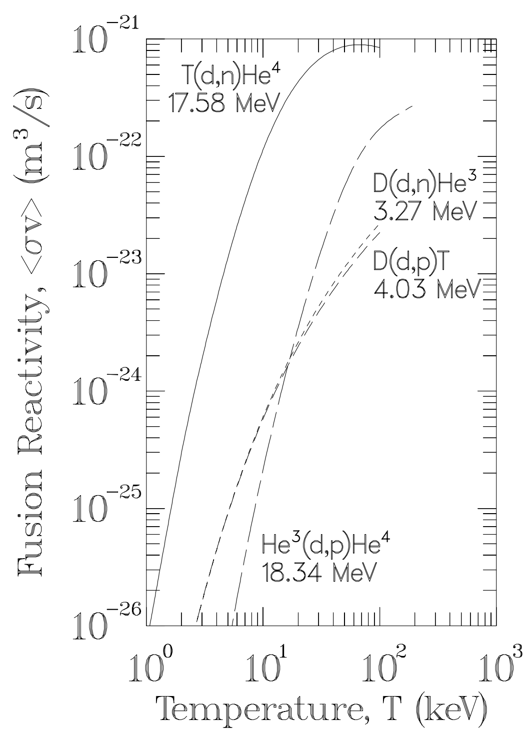

Figure 3.2-3. Temperature-dependent Maxwellian-averaged fusion reactivity, $\langle \sigma v \rangle_k$, for the various reactions listed in Table 3.2-III that are appropriate to SPPS/MHH.

Additionally, the charged-particle fusion-product power density in the power-balance model is related to the fusion power density in Eq. (3.2-21) by

$$p_{CP} \;=\; (1-f_p)\sum_k \frac{P_{Fk} f_{CP}}{V_p}\;; \qquad (3.2\text{-}23)$$

where f_p is the prompt fusion-product loss, f_{CP} is the fraction of the fusion power carried by charged fusion products, and the sum is over the k reaction given in Table 3.2-III.

The tritium-fuel source rate, S_T, in steady state balances the sum of the tritium burnup and loss rate, $L_T = f_t n_i/\tau_p$. Another plasma parameter that uses the profile-form factor for fusion reactions is the tritium burnup fraction, f_B, for DT systems and it is given by

$$f_B \;\equiv\; \frac{S_T - L_T}{S_T} \approx \left[1 + \frac{1}{g_{DT}\, f_D\, \langle\sigma v\rangle_{DT}\, n_i\, \tau_E\, \left(\tau_p/\tau_E\right)}\right]^{-1} . \qquad (3.2\text{-}24)$$

where $\langle\sigma v\rangle_{DT} \gg \langle\sigma v\rangle_{DD}$ is assumed. The particle confinement time, τ_p, is specified by a factor (4 for the SPPS/MHH) multiplied by the energy confinement time, tau_E. For the reference SPPS/MHH design, $f_B \simeq 0.095$, and the Lawson confinement parameter is $n_i\tau_E \simeq 2.55\times 10^{20}$ s/m^3.

Particle Balance. Assuming all ion species have the same particle confinement time, τ_p, the ion continuity equations are given by

$$\frac{n_\alpha}{\tau_p} \;=\; R_{\mathrm{DT}} + R_{\mathrm{D^3He}}\,, \qquad (3.2\text{-}25)$$

$$\frac{n_{\mathrm{P}}}{\tau_p} \;=\; R_{\mathrm{D^3He}} + R_{\mathrm{DDP}}\,, \qquad (3.2\text{-}26)$$

$$\frac{n_{\,^3\mathrm{He}}}{\tau_p} \;=\; -R_{\mathrm{D\,^3He}} + R_{\mathrm{DDN}} + \phi_{\,^3\mathrm{He}} S\,, \qquad (3.2\text{-}27)$$

$$\frac{n_{\mathrm{T}}}{\tau_p} \;=\; -R_{\mathrm{DT}} + R_{\mathrm{DDP}} + \phi_{\mathrm{T}} S\,, \qquad (3.2\text{-}28)$$

$$\frac{n_{\mathrm{D}}}{\tau_p} \;=\; -R_{\mathrm{DT}} - R_{\mathrm{D\,^3He}} - 2\,R_{\mathrm{DDP}} - 2R_{\mathrm{DDN}} + \phi_{\mathrm{D}} S\,, \qquad (3.2\text{-}29)$$

where R_{ij} is the fusion reaction rate per unit volume between species i and j [Eq. (3.2-22)], S is the total particle fueling rate per unit volume, and ϕ_j is the fractional composition of the fuel with $\phi_{\,^3\mathrm{He}} + \phi_{\mathrm{T}} + \phi_{\mathrm{D}} = 1$. The values of ϕ_{D} and ϕ_{T}, as well as the τ_p/τ_{E_e} ratio, are input to the ASC*. It was assumed that $\tau_p/\tau_{E_e} = 4$. The issue of recycling of fuel ions or fusion-product alpha particles across the interface between the plasma edge and the scrape-off layer has not been examined in detail.

An optimal 50:50 fuel mixture ($\phi_{\rm D} \simeq \phi_{\rm T} \simeq 0.5$) was used for the SPPS/MHH. The value of $\tau_p/\tau_{E_e} = 4$ gives a fractional burnup of ~10%; a higher burnup fraction would provide a lower tritium inventory. These τ_p/τ_{E_e} values were not forced to be self-consistent with either the assumed density and temperature profiles or any particle and energy transport models.

Power Balance. The steady-state, zero-dimensional ion and electron power balance equations, written in terms of power density, are given by

$$p_{CP_i} + p_{H_i} = p_{TR_i} + p_{ie} \, , \tag{3.2-30}$$

$$p_{CP_e} + p_{H_e} + p_\Omega + p_{ie} = p_{TR_e} + p_{BR} + p_{CY} + p_{LINE} \, . \tag{3.2-31}$$

The charged-particle fusion-product power density, p_{CP}, is calculated by summing over D^3He, DD, and DT fusion reactions [Eq. (3.2-23)]. The power density deposited in the ions and electrons, p_{CP_i} and p_{CP_e}, respectively, (assuming a specified prompt loss fraction, which is the same for all charged-particle fusion products) is calculated through a time integral of the slowing down rate of a test particle against the background ions over the time for the test particle to thermalize [9].

The heating power densities provided by sources external to the plasma are

$$p_{H_i} = \frac{p_{CP}}{Q_p} f_{H_i} \, , \tag{3.2-32}$$

$$p_{H_e} = \frac{p_{CP}}{Q_p}(1 - f_{H_i}) \, . \tag{3.2-33}$$

The fractional heating power going to the ions, f_{H_i}, is additional information provided with the heating power, and the plasma gain, $Q_p \equiv P_{CP}/P_H$, is a result of the convergence loop fixing the net electrical power. The term that partitions energy between the ions and electrons is given by p_{ie}.

The transport energy losses are characterized by ion and electron energy confinement times as follows:

$$p_{TR_i} = \frac{3}{2} k_B n_i \, T_i/\tau_{E_i} \, , \tag{3.2-34}$$

$$p_{TR_e} = \frac{3}{2} k_B n_e \, T_e/\tau_{E_e} \, . \tag{3.2-35}$$

where k_B is the Boltzmann constant (1.602×10^{-19} J/eV). The total transport energy confinement time is given by

$$\tau_E = \frac{n_i T_i + n_e T_e}{(n_i T_i/\tau_{E_i}) + (n_e T_e/\tau_{E_e})} \,, \tag{3.2-36}$$

and a ratio $\tau_{Ei}/\tau_{Ee} = 1$ is assumed. The plasma-energy confinement time expressed in terms of the net heating power, $P_{TR} \simeq P_{PH}(1 - f_{RAD})$, is

$$\tau_E = \frac{W_p}{P_{PH}\,(1 - f_{RAD})} \,; \tag{3.2-37}$$

where W_p is the total plasma kinetic energy, including the suprathermal fusion-product energy and any neutral-beam energy. The ASC* uses the particle- and power-balance calculations to establish the appropriate ion constituent fractions and the corresponding values of the Lawson parameter, $n_i\tau_E$, and τ_E. Once τ_E is known, a comparison can be made to any of a number of proposed empirical scaling laws. It should be emphasized that a scaling law is not used to derive any of the ARIES or SPPS design points; τ_E is determined from the specification of net electrical power and Q_p that is determined self-consistently with the power requirements of the (tokamak) current-drive system. The value of τ_E required for a design point can be compared to the various empirical scaling laws by means of a confinement multiplier, $H_j \equiv \tau_E/\tau_E^j$, where the subscript and superscript j denotes the particular scaling of interest.

Stellarator plasma energy confinement is seen to improve with density, magnetic-field strength, and volume, but degrades with input power; enhanced (H-mode) confinement has been observed in two devices. The global (L-mode) energy confinement time, τ_E, is given by (for example) the Lackner-Gottardi relation [10, 11]

$$\tau_E^{L-G} = 6.77 \times 10^{-10} R_T a_p^2 \bar{n}^{0.6} B_0^{0.8} P^{-0.6} \iota\!\!\!-^{0.4} \,, \tag{3.2-38}$$

where R_T (m) is the major toroidal radius, a_p (m) is the average plasma minor radius, $\bar{n}$ (10^{20} m^{-3}) is the line-averaged plasma density, B_0 (T) is the on-axis magnetic-field strength, P (MW) is the heating power, and $\iota\!\!\!-$ is the rotational transform (*i.e.*, the inverse of the tokamak safety factor, q). A possible enhancement factor, H, relative to Eq. (3.2-38) is monitored (*i.e.*, $H \simeq 2$ for H mode). Subsequent to the termination of technical work on the SPPS, a new International Stellarator Scaling (ISS95) has been proposed [12].

The radiation-loss channels for plasmas operating at temperatures above a few keV are Bremsstrahlung and cyclotron radiation. Impurities at these high temperatures are fully stripped of electrons and produce little line radiation. Impurities enhance plasma radiation by increasing the effective plasma charge. The electron-ion and electron-electron Bremsstrahlung local power density is given by [13]

$$\begin{aligned} p_{BR} &= 5.35\times10^{-43} n_e^2 Z_{eff} T_e^{\frac{1}{2}} \left[1 + 1.55\times10^{-3}\, T_e + 7.15\times10^{-6}\, T_e^2 \right. \\ &\left. + 4.14\times10^{-3}\, \frac{T_e}{Z_{eff}} + 0.071\, \frac{Z_{eff}^2}{T_e^{\frac{1}{2}}} \right] , \end{aligned} \tag{3.2-39}$$

which includes a correction for relativistic effects and uses the definitions of effective plasma charge and the effective square of the plasma charge given in Eqs. (3.2-4) and (3.2-5), respectively.

The cyclotron radiation global-power density, p_{CY}, for the SPPS/MHH is a relatively small loss, due to the modest magnetic field strength and reflective first-wall surface. Cyclotron radiation losses are a function of the effective first-wall reflectivity for cyclotron radiation, R_{CY}, which includes the effects of both reflection from the first wall and absorption in first-wall holes. The first-wall surface hole fraction for the SPPS/MHH is $f_H \simeq 0.10$, accounting promarily for the divertor channel openings. The cyclotron power lost through the divertor channels and other (smaller) holes in the first wall of the SPPS/MHH is about 2 MW.

The plasma-core radiation fraction is given by

$$f_{RAD} \equiv \frac{p_{BR} + p_{CY}}{p_{CP} + p_H + p_\Omega} . \tag{3.2-40}$$

The value of f_{RAD} for a DT plasma at $T \simeq 20$ keV with $Z_{eff} \simeq 1.5$ and a highly reflective ($P_{CY} \simeq 0$) first wall is $\simeq 0.5$, but drops below 0.2 at $T \simeq 10$ keV. The value for the SPPS/MHH reference case is $f_{RAD} = 0.21$.

No detailed calculations of the performance of the SPPS/MHH divertor system where performed. Relative to the ARIES tokamaks, the SPPS/MHH is expected to have fairly straightforward heat-removal rquirements. Attempts to improve upon the baseline SPPS/MHH case by increasing the power density can be expected to increase the loads on the high-heat flux surfaces. Any future, more detailed study should address this issue with greater care insofar as it may become performance limiting.

3.2.2. Power Plant Engineering

The ASC* model for reactor engineering characterizes the first wall, blanket, shield, coils, current-drive, and impurity-control hardware to provide the basis for the direct cost estimate of the FPC. Additionally, the plant power balance is modeled to size the balance-of-plant (BOP) requirements of the electric generating station.

The radial build of the SPPS/MHH configuration is summarized in Table 3.2-IV, consistent with the more detailed discussion found in Sec. 5. In common with the ARIES-II design, liquid-Li serves as both breeder and coolant and V5Cr5Ti serves as the structural material for the SPPS/MHH. The scale of the FPC for the MHH is to a large extent set

Table 3.2-IV.
SPPS/MHH Inboard Radial Build

SOL thickness, δ_s (m)	0.15
First wall:	
coating	none
composition	30% V5Cr5Ti, 70% Li
thickness (m)	0.014
Gap thickness (m)	0.
Blanket:	
composition	10% V5Cr5Ti, 90% Li
thickness (m)	0.350
Gap thickness (m)	0.020
Shield:	
composition	15% V5Cr5Ti, 5% Li, 80% Tenelon
thickness (m)	0.800
Gap thickness (m)	0.020
Cryostat (m)	0.100
Total thickness, δ_i (m)	1.454

by the restrictive inboard standoff as it interacts with the the necessity of protection of the coils from radiation damage.

The thermal-hydraulic properties of the liquid-metal blanket suggest [1] an adequate limit on the peak neutron wall load (≤ 10.4 MW/m^2), which is not encountered by typical SPPS/MHH design points, because of the interaction between the choice of plasma aspect ratio, plasma-coil standoff distance, design power level, *etc.*. The V-alloy coolant channels are assumed to be coated with an insulator (*e.g.*, CaO) to nullify the MHD contribution to the Li-coolant pumping power.

3.2.2.1. Magnetic Coils

The stellarator magnetic configuration is provided entirely by the external coil set. The specialized MHH coil configuration incorporates a nonplanar axis with four toroidal field periods, as illustrated in Fig. 3.2-1. Details of the coil internals are described in Sec. 4. For purposes of the ASC*, a homogenized characterization provides information regarding the coil masses and costs. The coil cross-sectional area is determined by the required magnetic field strength and a nominal overall coil current density of 30 MA/m^2. The homogenized coil mass density is taken to be 7,500 kg/m^3, ignoring variations in the structure-to-conductor ratio that can be expected across a parametric scan. The unit coil cost is taken to be a constant 98 $/kg, again ignoring expected dependancies, but including certain credits. This is the same unit coil cost used in the ARIES studies; no penalty for out-of-plane winding or other 'complications' attributed to the MHH configuration having been assessed. A limit on peak magnetic field strength at the coil windings was set at $\sim$14.5 T, lower than the 16-T limit imposed in the ARIES-II/IV cases. There is no convenient, general relationship describing the location of the peak coil field or scaling corresponding to the $1/R$ dependance of the toroidal-field strength in a standard tokamak. Thus, the MHH reference configuration can be scaled only in a restricted sense.

The ASC* includes models for continuous helical coils, consistent with the Large Helical Device (LHD) [14], presently under construction in Japan, or other proposed Compact-Torsatron (CT) configurations [3]. These models were not exercised in the course of the SPPS to perform a comparative assessment of modern stellarator configurations, as was done for an earlier study [15].

3.2.2.2. Thermal Cycle

The power recovered by the thermal cycle is divided into that deposited in the blanket, P_{TH}^{B}, and that delivered to the divertor, P_{TH}^{D}. The efficiency of converting the thermal blanket power to electricity is denoted by η_{TH}^{B}. The thermal-conversion efficiency for the divertor-coolant loop is denoted by η_{TH}^{D}, in order to model the case of a compound system (typically $\eta_{TH}^{D} < \eta_{TH}^{B}$) or the extreme case where the divertor power, P^{D}, is dumped to the environment as low-grade (waste) heat ($\eta_{TH}^{D} \simeq 0$). The power-to-wall area weighted-average thermal-conversion efficiency is defined as

$$\eta_{TH} = \frac{\eta_{TH}^{B}\, P_{TH}^{B} + \eta_{TH}^{D}\, P_{TH}^{D}}{P_{TH}^{B} + P_{TH}^{D}}\,, \tag{3.2-41}$$

where

$$P_{TH}^{B} = f_{RAD}\,(1-f_{D})\,(1-f_{DC})\,(P_{CP}+P_{H}+P_{\Omega}) + M_{N}^{DT}\,P_{N}^{DT} + M_{N}^{DD}\,P_{N}^{DD}\,; \tag{3.2-42}$$

$$P_{TH}^{D} = (1-f_{RAD}+f_{RAD}\,f_{D}\,(1-f_{DC}))\,(P_{CP}+P_{H}+P_{\Omega})\,. \tag{3.2-43}$$

In the above expressions, f_{RAD} is the core plasma-radiation fraction and is given by Eqs. (3.2-40); $f_{D} \equiv A_{D}/A_{FW}$ is the fraction of the first-wall surface area devoted to the divertor plate surfaces; f_{DC} is the fraction of the radiated power recovered for direct collection ($f_{DC} = 0$ for all ARIES designs); P_{CP} is the charged-particle fusion power; and M_{N}^{DT} and M_{N}^{DD} are the blanket neutron-energy multiplications for 14-Mev DT and 2.5-MeV DD neutrons, respectively. To avoid the design complication of two separate coolant circuits, the blanket and divertor use the same coolant inlet and outlet temperatures and pressures to yield $\eta_{TH}^{D} = \eta_{TH}^{B} = \eta_{TH}$. The thermal-cycle parameters used for the ARIES and SPPS/MHH designs are given in Table 3.2-V. The low-activation SiC blankets of ARIES-I and -IV result in the lowest energy multiplication for 14-MeV DT neutrons of the ARIES designs. However, the He-cooled ARIES-I and -IV designs have the highest thermal-conversion efficiencies.

The power flow, as modeled in the ASC*, is shown in Fig. 3.2-4 for the SPPS/MHH. Given a stipulated target for the net-electrical-power output, P_{E}, the thermal-power output, P_{TH}, is determined for a nominal value of the thermal conversion efficiency, η_{TH}, such that $P_{E} = \eta_{TH}(1-\epsilon)P_{TH}$, where $\epsilon = 1/Q_{E}$ is the recirculating power fraction and $Q_{E} \equiv P_{ET}/(P_{ET}-P_{E})$ is the engineering gain. The gross electrical power is $P_{ET} = \eta_{TH}P_{TH}$. A fraction $f_{AUX} = 0.04$ of P_{ET} ($P_{AUX} = f_{AUX}P_{ET}$) is allocated for auxiliary functions. A fraction f_{pump} of P_{ET} ($P_{pump} = f_{pump}P_{ET}$) is allocated for primary-loop pumping power. From Table 3.2-V, the gas-cooled ARIES-I and -IV designs require five

Table 3.2-V.
Thermal-Cycle Parameters of SPPS and ARIES Designs [1, 5]

	ARIES-I	ARIES-II	ARIES-IV	SPPS/MHH
Divertor coverage, $f_D \equiv A_D/A_{FW}$	0.25	0.15	0.15	0.15
Neutron Energy multiplication:				
14-Mev, M_N^{DT}	1.30	1.38	1.23	1.40
2.5-Mev, M_N^{DD}	4.20	3.70	4.27	3.70
Thermal conversion efficiency, η_{TH}	0.49	0.46	0.49	0.46
Pumping power fraction, f_{PMP}	0.05	0.01	0.05	0.01

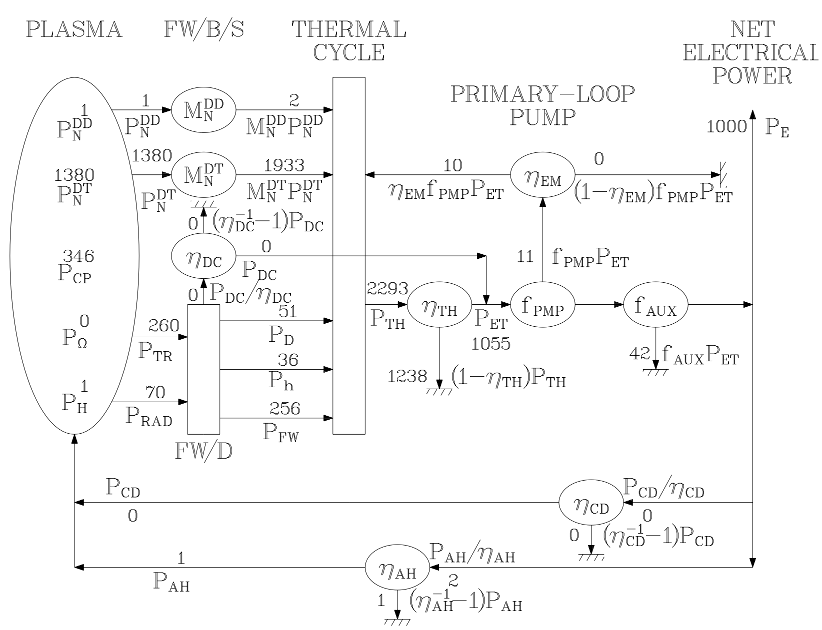

Figure 3.2-4. Overall power-flow diagram used in the ASC* for the SPPS/MHH. Values of powers are given in MW and are for the 1,000-MWe reference design. Powers with a superscript "*" denote discarded, low-grade heat.

times the pumping power of the liquid-cooled ARIES-II and SPPS/MHH designs. It is assumed that $0.98\,P_{pump}$ is recoverable as thermal power usable in the primary coolant loop; $0.9\,P_{pump}$ was assumed in ARIES-I [5]. The engineering gain, Q_E, can be written as

$$Q_E \;=\; \frac{1}{\epsilon} = \eta_{TH}\,\frac{M_N\,P_N + P_{CP} + P_H + P_\Omega + 0.98\,P_{pump}}{P_{AUX} + P_{pump} + \left(P_{CD} + P_{AH}\right)/\eta_{CD}}\,. \qquad (3.2\text{-}44)$$

The ratio of fusion power to external heating power is the plasma gain, $Q_p \equiv P_F/P_H$. For the SPPS/MHH, $Q_p \simeq 1,700$, consistent with a small external heating power (20 MW) to provide control at a steady-state operating point set slightly below ignition.

3.2.2.3. Neutron Wall Load

The average neutron first-wall load, $P_N/A_w = I_w$, is given by

$$I_w \;=\; \frac{0.8\,P_F^{DT} + 0.336\,P_F^{DD}}{4\pi^2\,R_T\,r_w}\,. \qquad (3.2\text{-}45)$$

A plasma filling fraction, $x \equiv r_p/r_w$, is calculated based on the assumed scrape-off layer thickness, $\delta_s = r_w - r_p$, taken to be 0.15 m for the SPPS/MHH. The poloidal distribution of the neutron wall load is calculated internal to the ASC*, as is shown in Fig. 3.2-5, corresponding to, but not representative of the actual 3-D MHH geometry, the results of the NEWLIT (tokamak) code [16]. Assuming toroidal symmetry, a three-dimensional neutron source (also shown in Fig. 3.2-5) is constructed from the volumes of the simulated flux surfaces and the radial profile of the neutron power density. The neutron wall load is calculated from approximate three-dimensional integrals over the source volume that has an unobstructed view of the wall, as determined by ray tracing. This calculation is repeated to construct the poloidal distribution of the neutron wall load that is shown in Fig. 3.2-5. Limiting values of peak neutron wall load $\hat{I}_w \geq 10.4$ MW/m^2 for ARIES-II or $\hat{I}_w \geq 5.8$ MW/m^2 for ARIES-IV were rejected for thermal-hydraulic reasons [1], but the former limit is not approached by the SPPS/MHH design using comparable self-cooled Li technology. The peak (local) neutron wall load, together with the assumed material fluence life, sets the service life of the module for purposes of scheduled changeout.

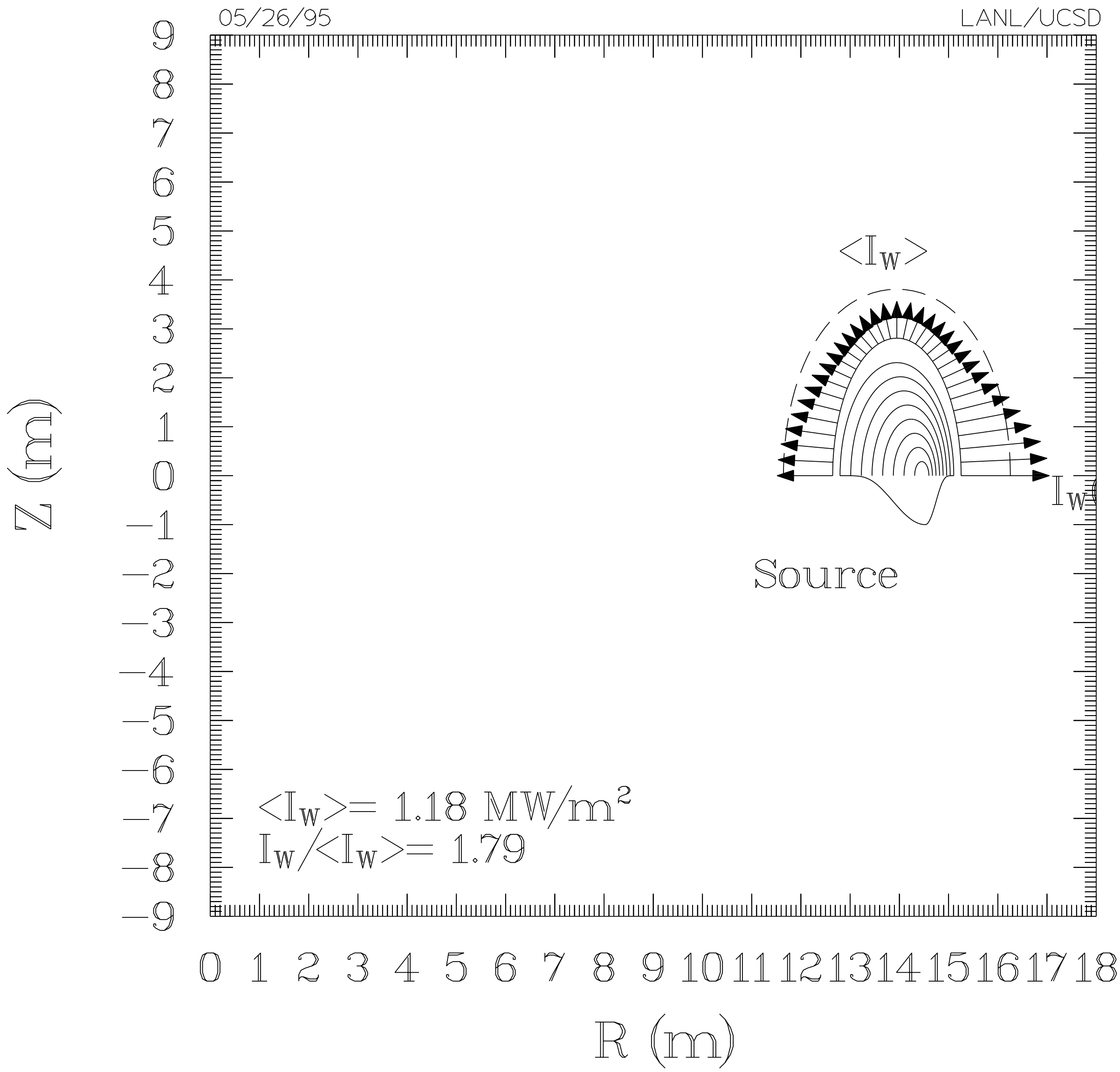

Figure 3.2-5. Schematic poloidal distribution of the neutron wall load for the SPPS/MHH, idealized consistent with the ASC* model, and not representative of any actual vertical cut through the MHH configuration. Also shown are the simulated flux surfaces used to construct the neutron source, the surface representing the first wall, and the neutron source in the equatorial plane as a function of major radius. Under these assumptions, the peak-to-average neutron wall load is $\hat{I}_w/I_w = 1.79$.

3.2.2.4. Fusion-Power-Core Mass

The total FPC mass, M_{FPC}, is the sum of coil, blanket, shield, and structure component masses. The ratio P_E/M_{FPC} (kWe/tonne) defines the FPC mass power density (MPD) figure of merit. A target value of ∼100 kWe/tonne has been identified as a necessary condition for a fusion power plant to be of marginal economic interest [17]. Higher power-density systems lead to higher values of MPD, with the MPD value that minimizes COE being highly dependent on the confinement concept [18, 19]. The value obtained for the SPPS/MHH is ∼47 kWe/tonne, which raises a concern that is somewhat mitigated in terms of its impact on the overall economics by the favorably low value of recirculating power. The low value of MPD is a direct result of the MHH geometry, as well as conservative assumptions regarding magnetic field strength, power density, and 14.1-MeV neutron wall load. The FPC mass is a distinguishing global characteristic, along with recirculating power fraction, in comparing various MFE point designs. FPC masses for several conceptual design are summarized in Table 3.2-VI. A representative Helias conceptual design, HSR20 [20], is also included.

Table 3.2-VI.
FPC Mass Parameter Comparison

	ARIES-II [1]	HSR20 [20]	SPPS/MHH
Masses (ktonne):			
First Wall, Blanket, Reflector	0.43	0.55	0.25
Shield	6.02	20.06	9.45
Coils:	2.41	13.36	4.19
TF coils	1.81		
PF coils	0.59		
Structure	1.23	1.10	5.36
Vacuum Vessel	0.71	2.20	2.17
Fusion Power Core, FPC	10.80	37.27	21.43
Mass Power Density, MPD (kWe/tonne)	92.6	26.5	46.7

3.2.3. Costing

3.2.3.1. Direct Cost Database

The ASC⋆ plasma and engineering models combine to provide a characterization of MHH power plants that is adequate for conceptual cost projections. Despite the uncertainty in projecting the future costs of an emerging and complex technology, a competitive cost, together with favorable safety and environmental characteristics, remain as important considerations in the eventual decision to commercialize fusion power [18, 19, 21]. This subsection reports the cost basis and methodology used in the SPPS. The ARIES/SPPS cost data base as used in the ASC⋆ is summarized on Table 3.2-VII. The direct-cost account entries, C_i, are obtained by applying relevant (installed) unit-cost estimates (*e.g.,* \$/W, \$/kg, \$/m^3) to the calculated usage of these items in the conceptual design, such that $C_i(\$) = u_i(\$/\text{unit})X_i$ (unit). A learning-curve or mass-production credit is taken for a "tenth-of-a-kind" commercial reactor installation, consistent with U.S. fusion-reactor design-community practice. The SPPS study, like STARFIRE [22] and most other U.S. fusion-reactor designs reported in the last decade, assumes FPC unit costs consistent with these learning-curve [23, 24] credits, rather than "first-of-a-kind" unit costs (including R&D) appropriate for the International Thermonuclear Experimental Reactor (ITER) [25]. A "80% learning curve" (*i.e.,* 0.80 progress ratio, p), as used for the ARIES tokamaks and the SPPS/MHH, represents the expectation [26], that each doubling of production represents a $p \simeq 0.8$ reduction in unit costs. A "tenth-of-a-kind" reactor represents, nominally, ∼3.3 doublings of production or $p^{(ln10/ln2)} \simeq 50\%$ cost reduction relative to "first-of-a-kind" FPC costs. Of course, actual production experience varies [24]. Learning credits are not applied to BOP items, consistent with mature industrial production in which the learning credits have already been wrung out. For similar reasons, a 94% learning curve is recommended for advanced fission cost estimates [27]. Because of the larger leverage of the stellarator FPC cost, relative to a tokamak, a more conservative learning-curve credit, as recommended in Ref. [29], would tend to penalize the stellarator preferentially.

The cost data base consists of cost scaling relationships of the general form

$$C_j\,(\$) \;=\; c_j\,(X_j)^{e_j}\,, \tag{3.2-46}$$

where X can be either a descriptive variable (*e.g.,* power, mass, volume) or a scaled variable, X_j/X_{REF}, related to a reference value, X_{REF} of X_j, and e_j is an appropriate

Table 3.2-VII.
Summary of ASC/ASC* Cost Data Base[(a,b,c)]

Acct. No.	Account Title	Cost (M$, 1992)
20.	**Land and Land Rights**	10.44
21.	**Structures and Site Facilities**	
21.1	Site improvements and facilities	18.44
21.2	Reactor building[(c)]	$77.1\,(V_{RB}/80,000)^{0.62}$
21.3	Turbine building	$28.67\,(P_{ET}/1200)^{0.75} + 5.72$
21.4	Cooling structures	$11.67\,(P_{ET}/1000)^{0.3}$
21.5	Power supply and energy storage bldg.	14.98
21.6	Miscellaneous buildings	125.10
21.7	Ventilation stack	2.96
22.	**Reactor Plant Equipment (RPE)**	
22.1	Reactor equipment	
22.1.1	First Wall/Blanket/Reflector:	
	Breeding material:	Table 2.2-VIII of Ref. [1]
	Liquid metal (LM): PbLi[(d,e)]	(see Acct. 26.1.)
	Li[(d,f)]	(see Acct. 26.1.)
	Water solution: $LiNO_3$[(d,g)]	$(12.81 f_{6_{Li}} + 4.02) \times 10^{-3}\, M$
	Blanket and first-wall structure	Table 2.2-VIII of Ref. [1]
	Be multiplier[(g)]	Table 2.2-IX of Ref. [1]
22.1.2	Shield	Tables 2.2-VIII & 2.2-IX of Ref. [1]
22.1.3	Magnet coils:	
	Superconducting	Table 2.2-XI of Ref. [1]
	Resistive Cu	Table 2.2-XI of Ref. [1]
22.1.4	Supplemental heating systems	Table 2.2-XII of Ref. [1]
22.1.5	Primary structure and support	$0.1840\, V_{STR}$
22.1.6	Reactor vacuum system	$0.024\, M_{VAC}^{(f)} + 4.09$ (kg/d)

Table 3.2-VII (Cont'd)

Acct. No.	Account Title	Cost (M$, 1992)
22.1.7	Power supply (switching, energy storage):	
	Superconducting PF coils	485.2 $\$/(\text{kVA})^{0.8}$
	Resistive-Cu coils	30.33 $/kVA
	Superconducting TF coils	60.66 $/kVA
	IBC$^{(f)}$	60.66 $/kVA
	OFCD$^{(f,g)}$	60.66 $/kVA
	Other	1.64
	TF IBC busbars$^{(f)}$	4.96
	DF IBC busbars$^{(f)}$	2.66
22.1.8	Impurity control system	
	TITAN	$0.108\,A_{DIV}$
	ARIES	$0.073\,A_{DIV}$
22.1.9	Direct energy conversion	Table 2.2-XIII of Ref. [1]$^{(h)}$
22.1.10	ECRH breakdown system	2.60
22.2	Main heat-transfer system:	
22.2.1	Primary coolant$^{(i)}$:	
	Li$^{(f)}$, PbLi, He	$233.9\,(P_{TH}/3500)^{0.55}$
	OC, $H_2O^{(g)}$	$75.0\,(P_{TH}/3500)^{0.55}$
22.2.2	Intermediate coolant system	$40.6\,(P_{TH}/3500)^{0.55}$
22.2.3	Secondary coolant system	$75.0\,(P_{TH}/3500)^{0.55}$
22.3	Auxiliary cooling systems	$1.10 \times 10^{-3}\,P_{TH}$
22.4	Radioactive waste treatment	$1.96 \times 10^{-3}\,P_{TH}$
22.5	Fuel handling and storage	
22.5.1	Pellet injectors	6.07 M$ each $\times 2$
22.5.2	Fuel processing system	$0.82\ (\text{g/d})^{0.7}$
22.5.3	Fuel storage	6.07
22.5.4	Atmospheric tritium recovery	$0.33\ (\text{m}^3/\text{h})^{0.6}$
22.5.5	Water detritiation system:	
	TITAN-I, ARIES-I	8.18
	TITAN-II	229
22.6	Other reactor plant equipment	$1.78 \times 10^{-3}\,P_{TH}$
22.7	Instrumentation and control	38.29

Table 3.2-VII (Cont'd)

Acct. No.	Account Title	Cost (M$, 1992)
23.	**Turbine Plant Equipment**$^{(i)}$	
	OC, H_2O	$254.4\ (P_{ET}/1200)^{0.83}$
	Li, PbLi	$240.3\ (P_{ET}/1200)^{0.83}$
	He	$205.5\ (P_{ET}/1200)^{0.7}$
23.1	Turbine generators	
23.2	Main steam system	
23.3	Heat rejection systems	
23.4	Condensing system	
23.5	Feed heating system	
23.6	Other turbine plant equipment	
23.7	Instrumentation and control	
24.	**Electric Plant Equipment**$^{(i)}$	$126.4\ (P_{ET}/1200)^{0.49}$
24.1	Switchgear	
24.2	Station service equipment	
24.3	Switchboards	
24.4	Protective equipment	
24.5	Electrical structures and wiring containers	
24.6	Power and control wiring	
24.7	Electrical lighting	
25.	**Miscellaneous Plant Equipment**$^{(i)}$	$60.5\ (P_{ET}/1200)^{0.59}$
25.1	Transportation and lifting equipment	
25.2	Air and water service systems	
25.3	Communications equipment	
25.4	Furnishings and fixtures	
26.	**Special Materials**	
26.1	Reactor LM coolant/breeder:$^{(d)}$	
	PbLi$^{(e)}$	$(12.81 f_{^6Li} + 4.02) \times 10^{-3} M_{LM}$
	Li$^{(f)}$	$(1233 f_{^6Li} + 61.2) \times 10^{-3} M_{LM}$
26.4	Other	0.41
26.5	Reactor-building cover gas $^{(f,j)}$	0.21

Table 3.2-VII (Cont'd)

Acct. No.	Account Title	Cost (M$, 1992)
90.	**Total Direct Cost (TDC)**	
91.	**Construction Services and Equipment**	Table 3.2-VIII
92.	**Home Office Engineering and Services**	Table 3.2-VIII
93.	**Field Office Engineering and Services**	Table 3.2-VIII
94.	**Owner's Cost**	Table 3.2-VIII
95.	**Process Contingency**	Table 3.2-VIII
96.	**Project Contingency**	Table 3.2-VIII
97.	**Interest during Construction (IDC)**	Table 3.2-X
98.	**Escalation during Construction (EDC)**	Table 3.2-X
99.	**Total Capital Cost (TCC)**	

$^{(a)}$ Adapted from Table 2.3-VII of Ref. [5] and Table 2.2-XV of Ref. [1].
$^{(b)}$ Installed cost (LSA = 4), including future learning credits for a tenth-of-a-kind plant.
$^{(c)}$ Gross electrical power, P_{ET}, net electrical power, P_E, and total thermal power, P_{TH}, are given in MW. Volumetric V (m^3) or corresponding mass M (tonne) unit costs for the FPC and related items are given as follows:
Reactor building, $V_{RB} = 4\,(R_T + r_s + 9)^2 (f_z r_s) + 1.50 \times 10^5 + 150\ P_{CD}^{NBI}$;
Blanket, M_{BL} ; Shield, M_{SHD};
Magnet coils, M_C; Structure, V_{STR}; Vacuum tank, M_{VAC};
Divertor-plate surface area, A_{DIV} (m^2).
$^{(d)}$ Liquid metal, M_{LM} (tonne): ^{6}Li enriched, $0.075 < f_{^6Li} < 0.90$ [30].
$^{(e)}$ Applicable to CRFPR [31] and MARS [32].
$^{(f)}$ Applicable to TITAN-I [33].
$^{(g)}$ Applicable to TITAN-II [33].
$^{(h)}$ 0.32 $/W for ARIES-III/FSR [34] case only.
$^{(i)}$ Ref. [35].
$^{(j)}$ Applicable to ARIES-I [5].

scaling exponent (usually $0 < e_j < 1$). Equation (3.2-46) can be rewritten in the form

$$C_j \;=\; \frac{c_j\,(X_j)^{1-e_j}\;(X_j)^{e_j}}{(X_j)^{1-e_j}} \;=\; \left[\frac{c_j}{(X_j)^{1-e_j}}\right] X_j \;, \tag{3.2-47}$$

which allows the definition of a (variable) unit cost

$$u_j \;=\; \frac{c_j}{(X_j)^{1-e_j}} \;, \tag{3.2-48}$$

and is a dependent function of the descriptive variable, X_j, itself. While the cost accounting scheme allows for detailed cost breakdowns (to four levels), only a two-level subset of items is estimated and reported explicitly for their conceptual reactor design. The cost scaling exponents, e_j, used for the ARIES series and the SPPS are typically consistent with those of the U.S. fission-reactor experience [28] and represent the inclusion of quality-control costs associated with nuclear-safety-grade (N-stamped) components.

Minimal effort was devoted to architectural/engineering (AE) issues relating to the SPPS/MHH plant layout, as well as building design and costing. The reactor-building elevation and plan views depicted on p. 20-95 to 20-98 of the STARFIRE report [22] are considered relevant to ARIES-tokamak and SPPS/MHH applications. The MFE reactor building is a (large) rectangular ribbed-box structure subdivided into a reactor hall and a "process-module room" containing the primary coolant loop and other support systems. The reactor-building reinforced-concrete walls and roof have a thickness of 1.5 m for seismic, tornado-missile, and radiation-shielding reasons; the building is steel-lined to contain tritium. The interior layout assumes fully remote maintenance and contains a 600-tonne-capacity overhead bridge crane. The floor of the reactor hall and process-module room is at grade level, supported by a 16-m high subgrade structure and pipe chase. The volume of the process-module room is retained as a fixed contribution of 1.5×10^5 m^3, to which is added a 15% increment for an intermediate coolant loop (ARIES-II and SPPS/MHH), to which is added volume for neutral-beam injection (NBI, ARIES-III only), based on the scaling $V_{NBI} = 150 P_{NBI}$, where V_{NBI} is in m^{-3} and P_{NBI} (MW) is the NBI power. The reactor hall scales with the size of the FPC envelope and has differing peripheral and overhead clearance requirements based on the choice of either horizontal or vertical remote maintenance. Horizontal maintenance is adopted for the SPPS/MHH. The reactor building volumes, V_{RB}, for ARIES-I, -II, -III, and -IV are 1.96×10^5, 2.18×10^5, 2.30×10^5, and 2.03×10^5 m^3, respectively. The corresponding building volume for the SPPS/MHH is 2.33×10^5 m^3. Other buildings are taken to be fixed costs (*cf.*, STARFIRE [22]), including 14.98 M$ for the power-supply building, and 124.62 M$ for miscellaneous buildings (including 87.77 M$ for the hot-cell building). The cost of the

Turbine building (TB) is scaled [36] by $C_{21.3} = C_{TB}$ (M\$) $= 28.67(P_{ET}/1,200)^{0.75} + 5.72$, where the second term represents "fixed" building services and architectural costs (*cf.*, STARFIRE [22]).

3.2.3.2. LSA Credits

Potential cost savings derived from the substitution of conventional (non-nuclear) components, as well as the elimination of certain active safety systems or other excess components [37, 38], under the condition of demonstrable inherent safety are significant, but controversial [39]. Cost differentials between fission and coal plants reflect both quality assurance requirements and distinct considerations related to extreme loads (*e.g.*, seismic, missiles, *etc.*) [40]. Investment protection considerations may inhibit taking full advantage of possible credits. Cost credits represent both the simplifications resulting from the elimination of active safety systems as well as the assumed reduction in costs associated with the quality assurance requirements mandated in the U. S. by Appendix B of 10CFR50 [*i.e.*, the substitution of conventional for nuclear-safety-grade (N-stamped) components]. Detailed bulk-commodity and labor costs for N-stamped *versus* conventional construction are described in Sec. 2.3 of Ref. [27]. The safety assurance credit factors used for the ARIES-I study (*cf.* Table 2.3-VI of Ref. [5]) have been superseded for the present study by a new set of credits associated with the various Levels of Safety Assurance (LSA) [41–43], which provide progressive discounts relative to nuclear-safety-grade (LSA = 4) costs to credit passive safety down to conventional (LSA = 1, coal plant) costs for certain cost subaccounts. Following Piet [41] and ESECOM [42], LSA = 4 denotes active protection (*i.e.*, active engineered safety systems are required); the system does not meet the minimum requirements for inherent safety. For LSA = 3, safety is assured by passive mechanisms of release limitation as long as severe violations of small-scale geometry (*e.g.*, large coolant pipe breaks) are avoided. For LSA = 2, safety is assured by passive mechanisms as long as severe reconfiguration of large-scale geometry is avoided. For LSA = 1, safety is assured by passive mechanisms of release limitation for any accident sequence; radioactive inventories and material properties preclude a fatal release regardless of the reactor's condition. The postulated LSA cost-credit factors [43] are summarized in Table 3.2-VIII.

3.2.3.3. Financial Assumptions

The economic models used for the ARIES tokamaks and the SPPS/MHH are largely consistent with updates [48] made to the GENEROMAK [46, 51] models, incorporating,

Table 3.2-VIII.
Level of Safety Assurance (LSA) Cost-Credit Factors[a]

LSA:	1	2	3	4
Blanket[b]	0.90	0.95	1.0	1.0
Shield[b]	0.90	0.95	1.0	1.0
Coils[b]	0.90	0.95	1.0	1.0
Reactor & hot-cell buildings	0.60	0.90	0.96	1.0
Other structures and improvements	0.60	0.67	0.67	1.0
Heat transfer and transport	(*c*)	1.0	1.0	1.0
Other Reactor Plant Equipment	0.85	0.94	0.94	1.0
Turbine Plant Equip. & building	1.0	1.0	1.0	1.0
Electrical Plant Equipment	0.75	0.84	0.84	1.0
Miscellaneous Plant Equipment	0.85	0.90	0.93	1.0
Heat reject system	1.0	1.0	1.0	1.0
Land	1.0	1.0	1.0	1.0
All other direct cost areas	1.0	1.0	1.0	1.0
Indirect costs, Acct. No.:				
91. Constr. Ser. & Equip.[d]	0.113	0.120	0.128	0.151
92. Home Off. Engr. & Ser.[d]	0.052	0.052	0.052	0.052
93. Field Off. Engr. & Ser.[d]	0.052	0.060	0.064	0.087
94. Owner's Cost[e]	0.150	0.150	0.150	0.150
95. Process Contingency[f,g]	NA	NA	NA	NA
96. Project Contingency[f]	0.150	0.173	0.184	0.195
O&M costs[h]	0.70	0.85	0.925	1.0
D&D allowance, $C_{D\&D}$ (mill/kWeh):				
nominal $	0.38	0.75	1.13	1.50
constant $	0.25	0.50	0.75	1.00

[a] Multiplicative factor applied to cost model accounts, *cf.* Refs. [35, 43], superseding Table 2.3-VI of Ref. [5].
[b] *cf.* Refs. [5, 44–46].
[c] 0.60 for liquid metal or other cooling system requiring an intermediate heat exchanger (IHX) or a helium or other cooling system requiring a double-walled steam generator with LSA = 4; 0.90 otherwise.
[d] factor $\times [TDC]$
[e] factor $\times [TDC + C_{91} + C_{92} + C_{93}]$
[f] factor $\times [TDC + C_{91} + C_{92} + C_{93} + C_{94}]$
[g] Not applied to a mature, tenth-of-a-kind commercial plant.
[h] from Eq. (3.2-52), also see Ref. [47].

for example, a lowering of the federal income tax rate from 46% to 34% under provisions of the U.S. Tax Reform Act of 1986. The discount rate influences societal choices by reflecting economic risk and weights the present rather than future consumption. Generally, a high discount rate penalizes capital-intensive projects (*e.g.*, fusion and fission relative to coal) and can reverse the advantages provided by lower fuel costs. The financial parameters assumed here are consistent with those of U. S. utilities; industrial or Independent-Power-Producer (IPP) ownership of the power plant results in significantly higher cost of money, as shown in Table 3.1. of Ref. [27]. The resulting impact on the COE of a typical tokamak power plant is severe enough, as shown in Table 1 of Ref. [49], with the COE for the same plant ascribed to a non-utility generator (NUG) projected to be 37% – 50% higher. A similar penalty is expected for a stellarator power plant. Thus, non-utility ownership of a capital-intensive fusion power plant is not likely. The economic parameters assumed in the costing model used in the ARIES and SPPS/MHH studies are summarized in Table 3.2-IX.

The detailed methodology for calculating the time-related cost factors is described in Refs. [51] and [52]. This description differs from the U.S. fusion-reactor-community standards [53, 54] used in the period 1980 to 1985 because a slightly different "s-shaped" spending profile during construction is assumed. A more precise spending profile could be derived from a detailed construction schedule and historical experience, as has been attempted in the past for fission systems [55], consistent with the present approximation, but such an effort is not justified by the level of detail of the ARIES and SPPS/MHH conceptual designs. The reference design and construction lead time, τ_c, for the ARIES tokamaks and SPPS/MHH conceptual power plants is assumed to be six years, consistent with the STARFIRE study [22] and projections for advanced fission systems that would be licensable and accepted by the public. Such a schedule assumes factory fabrication and timely delivery of modular FPC components. The critical path in the reference schedule (*cf.* Fig. 23-1. of Ref. [22]) is determined by construction of the reactor building and installation of the FPC. Development of more detailed algorithmic construction schedules, which might be expected to penalize larger or more complex systems, was beyond the scope of the ARIES study and the SPPS effort, as well. Standard assumptions regarding construction time ($\tau_c = 6$ y), plant capacity factor ($p_f = 0.76$), economies of scale, and operations and maintenance (O&M) charges are used to estimate the constant-dollar (1992) COE. Without developing a detailed construction schedule, the construction lead time is taken to be six years, which is in common with the lead times of the STARFIRE [22], MARS [32], TITAN [33], and ARIES [1, 5] studies.

Table 3.2-IX.
Reference Economic Parameters[a]

Plant life (analysis period), N (yr)	30
Plant lead (construction) time, τ_c (yr)	6
Indirect and Contingency cost factors	[b]
Factor for interest during construction, f_{IDC}:	
Nominal $	0.2630
Constant $	0.1652
Factor for escalation during construction, f_{EDC}:	
Nominal $	0.2335
Constant $	0.0
Assumed plant capacity factor, p_f	76%
Factor for spares[c], Acct. No.:	
21-23.98.	0.02
24.98.	0.04
25.98.	0.03
26.98.	0.00
Average cost of money[d], x_{COM} (/yr):	
Nominal $	0.1135
Constant $	0.0605
Effective tax-adjusted cost of money (discount rate), X (/yr):	
Nominal $, X	0.0957
Constant $, X_0	0.0435
Inflation rate, y (/yr)	0.05
Effective state and federal tax rate, t (/yr)	0.3664
Local property tax rate (/yr)	0.02
Tax depreciation life (yr):	
Overall plant	15
Replaceable blankets, *etc.*	5
Fixed charge rate, FCR:	
Nominal $, FCR	0.1638
Constant $, FCR_0	0.0966
Interim annual replacement rate, RR (/yr)	0.005

[a] *cf.* Ref. [46], Table 3.1., as updated (*cf.* Refs. [48, 50]).
[b] LSA dependence (*cf.* Table 3.2-VIII.).
[c] *cf.* Ref. [22].
[d] Allowance for Funds Used During Construction (AFUDC) rate.

Cost of electricity, COE (mill/kWeh), estimates are somewhat sensitive to construction time through the time-dependent interest (for constant $) or interest and escalation (for nominal-dollar) factors, summarized on Table 3.2-X. Following the discussion in Appendix D.IV of Ref. [51], the factor for interest during construction, f_{IDC}, is calculated for a representative construction (spending) profile, and the factor for nominal-dollar escalation during construction, $f_{EDC} = f_{cap} - f_{IDC}$.

Table 3.2-X.
Time-Related Economic Factors[a]

Lead Time (yr)	Constant $		Nominal $	
	f_{IDC}	$f_{EDC} = 0$	f_{IDC}	f_{EDC}
3	0.0863		0.1624	0.0951
4	0.1118		0.2119	0.1394
5	0.1381		0.2637	0.1887
6[b]	0.1652		0.3178	0.2436
7	0.1931		0.3743	0.3045
8	0.2219		0.4332	0.3719
9	0.2515		0.4948	0.4466
10	0.2821		0.5591	0.5291
11	0.3136		0.6263	0.6201
12	0.3460		0.6964	0.7206
13	0.3795		0.7696	0.8312
14	0.4139		0.8461	0.9530
15	0.4495		0.9261	1.0869

[a] compare with Table 22-54. of Ref. [22].

[b] Reference construction lead time, τ_c.

3.2.3.4. Cost of Electricity

The COE is the most important evaluation tool for optimizing and comparing with alternative energy sources. Both constant-1992 and nominal- or then-current-1998 dollar analyses (consistent with the assumed six-year design and construction lead time, τ_c) are used to evaluate the projected costs. Constant-dollar cost is defined as the cost measured in dollars that have a general purchasing power as of some reference date, while nominal- (current or as-spent) dollar costs include inflation [27]. The projected busbar energy cost is given by

$$\mathrm{COE} \;=\; \frac{C_{AC} + (C_{O\&M} + C_{SCR} + C_F)\,(1+y)^Y}{8760\,P_E\,p_f} + C_{D\&D}\,, \qquad (3.2\text{-}49)$$

where COE (mill/kWeh) is Cost of electricity in constant or nominal (then- current) dollars; C_{AC} is the annual capital cost charge, equals the total capital cost (TCC) multiplied by the fixed charge rate (FCR); C_i is the cost of account i; $C_{O\&M}$ is the annual operations and maintenance cost, ($C_{O\&M} = C_{40} + C_{41} + \ldots + C_{47}$); C_{SCR} is the annual scheduled component-replacement cost, ($C_{SCR} = C_{50} + C_{51}$); C_F is the annual fuel costs, C_{02}; y is the annual escalation rate; Y is the construction period (in year); P_E is the net plant electrical power (MWe) or Design Electrical Rating (DER); p_f is the plant capacity factor; TDC is the total direct cost (TDC $= \sum_{i=20}^{26} C_i$); C_{IDC} is the interest during construction ($C_{97} = f_{IDC}\,$TDC, *cf.* Table 3.2-X); C_{EDC} is the escalation during construction ($C_{98} = f_{EDC}\,$TDC, *cf.* Table 3.2-X); TCC is the total capital cost (TCC $= \sum_{i=20}^{98} C_i$); and $C_{D\&D}$ is the decontamination and Decommissioning (waste disposal) allowance.

Because of possible erosion and neutron damage, plasma facing components and the blanket structure are periodically replaced on a scheduled basis independent of possible repair/replacement due to unscheduled failures. In this regard, these nonpermanent components are analogous to the fuel elements in a fission reactor, leading the GENEROMAK study [46, 56] to exclude the cost of these items from the direct cost of the FPC. Such an approach, while understandable and conceptually consistent with fission industry practice, when applied to fusion systems where these items represent a larger fraction of the cost of the FPC, leads to a misleading (in the view of the ARIES Team) underestimate of the direct cost of the FPC. Therefore, following the practice of the STARFIRE [22], TITAN [33], and ARIES [1, 5] studies, such items are included in the direct costs. The ARIES-I study [5] did not amortize the cost of replaceable blanket sectors over their individual periods of service, as recommended by Ref. [46]. For the recent ARIES-II/IV study [1] and present SPPS, an appropriate calculation of the annual cost of the present worth of the revenue requirement for the investment in components which have a service period, $L = I_w\tau/\hat{I}_w$, that is, the neutron-fluence lifetime divided by the peak neutron wall load. Following Eq. (3.7) of Ref. [46], the present worth, F, of the revenue requirements for a unit investment that is depreciated for tax purposes over a period, T, is given by

$$F = \frac{1}{(1-t)}\left[1 - t\sum_{n=1}^{T}\frac{d_n}{(1+x)^n}\right], \tag{3.2-50}$$

where $t = 0.3664$ yr^{-1} is the effective tax rate, d_n is the fraction of the cost which is deductible for tax purposes in year n after investment, and $x = 0.1135$ is the nominal-dollar cost of money from Table 3.2-IX. For the scheduled replacement items of the FPC, a $T = 5$ year depreciation schedule is used, *cf.* Table 2 of Ref. [48] and Table 2.6. of Ref. [50], resulting in $F = 1.272$. Thus, the appropriate term in Eq.(3.2-49) becomes

$$C_{SCR} \propto (C_{21.1.1} + C_{22.1.8})CRF(X_0, L)F(1 + f_{96})/L\,, \tag{3.2-51}$$

where the contingency cost factor, f_{96}, from Table 3.2-VIII has been included. No additional engineering indirect costs are applied. For an assumed first-wall neutron fluence life $I_w\tau = 16.4\,\mathrm{MW\ yr/m^2}$ at a cost-optimized peak neutron wall load of $\hat{I}_w \simeq 2.11\,\mathrm{MW/m^2}$ and a plant capacity factor $p_f \simeq 0.76$, routine (scheduled) replacement of the first wall and blanket occurs every 7.8 full-power years or 10.2 calendar years. The cost of used (spent) blanket disposal is assumed to be part of the decontamination and decommissioning cost. No explicit credit has been taken for recovery/recycling of blanket material, although this is a recognized, but perhaps minor, cost-savings measure.

The cost of scheduled component replacement is separate from the annual operations and maintenance charge (Acct. 40.–47., 51.). The O&M cost was previously estimated [53, 57] to be ~2% of the direct cost, assessed annually; the present projection is approximately 1.8% of the direct cost. The O&M cost is scaled, together with its LSA factor from Table 3.2-VIII, by [47]

$$C_{O\&M}\,(\mathrm{M\$/y}) = 74.4\,(P_E/1200)^{0.5}\,, \tag{3.2-52}$$

for the ARIES-II/IV and SPPS/MHH studies. This revised projection is ~6% higher than that used for the ARIES-I study [5, 58]. This O&M cost, strictly speaking, depends on system complexity and the requirements of regulations, security, and maintenance, such that there may, in fact, be discernable differences between tokamaks and stellarators not identified or credited (one way or the other) because of the use of this simplifying power scaling.

The SPPS/MHH power plant is assumed to have a 30-yr service life and an average plant capacity factor, $p_f = 0.76$, corresponding to 22.8 full-power years. At the end of the tenth and twentieth years of operation, an extended outage of 120 days is anticipated for turbine generator overhaul and concurrent superconducting TF-coil anneal (if necessary), resulting in a contribution of 8 days to the annual scheduled downtime. Additionally, 28 days per year are allocated for routine scheduled outages, including the replacement of FPC FW/blanket modules. For unscheduled outages, 52 days per year are budgeted, leading to a total downtime of 88 days per year, corresponding to $p_f = 0.76$. A detailed allocation of downtimes for maintenance and/or replacement among subsystems has not been made.

Cost projections made for the fission industry [56] use a similar capacity factor, which is a target that has been exceeded by individual plant experience, but which is beyond the recent U.S. fission industry average of 69.3% [59]. Projections as high as 90% for the availability and 85% for the corresponding capacity factor of advanced (future) fission systems have been made [37]. The capacity factor is often less than the availability factor, reflecting regulatory restriction or load following. The higher complexity and size (mass) of fusion systems components may imply an availability penalty relative to fission systems. As seen from Eq. (3.2-49), the value of p_f affects the projected COE hyperbolically.

In parametric studies, the plant capacity factor has been assumed to be independent of the plant size (*i.e.*, P_E). Although ambiguous evidence [60] from the fission industry exists that p_f decreases with increasing P_{ET}, this trend is not seen in more recent U.S. fission experience [61]. Such an effect, if present, inhibits attempts to exploit "economies of scale" by pushing to larger plant sizes as a means to decrease COE values [62].

The fuel cost, C_F, of deuterium for is represented by Account 02. The unit cost of deuterium as D_2 is 3,700 \$/kg [22, 57]; deuterium contributes negligibly to the COE of a fusion power plant. In the long run, the power plant is self-sufficient in terms of tritium fuel production because of the breeding capability of the blanket so that no specific tritium-fuel charge is reported. It should be recognized, however, that a significant "hidden" cost for tritium exists in the direct cost of the DT fueled fusion reactor (*i.e.*, thicker, more complex tritium breeding blanket with thermal-hydraulic constraints not encountered soley by heat-recovery requirements).

3.3. DESIGN POINT SELECTION

The SPPS/MHH reference design is selected to meet simultaneously 1) the geometric constraint imposed by the incorporation of a minimal blanket/shield standoff distance into the scaleable reference MHH plasma/coil configuration, 2) a technology limit on peak magnetic field strength at the coil, and 3) a target net electrical power output of 1,000 MWe. The latter point is somewhat arbitrary, but facilitates certain cost comparisons with the ARIES tokamak power plant designs. It should be noted that such design decisions taken at the conceptual level might mask significant differences in performance and cost that could arise by exploiting the unique features of one approach relative to the other.

3.3.1. Plasma Physics

Physics parameters of the SPPS/MHH reference design are summarized in Table 3.3-I in comparison with those of ARIES-II [1]. The tokamak performance optimization leads to lower plasma beta in order to reduce the current-drive power requirement. Thus, the MHH beta value used here exceeds that of the tokamak. Absent a scaling relating the beta value to plasma aspect ratio or profile parameters, for example, the SPPS/MHH physics parameters should be considered as representative, but not necessarily optimized in the global context of the design point. Operating at comparable plasma temperatures (~10 keV), the SPPS/MHH plasma density is somewhat lower, consistent with the lower confining magnetic field. The plasma volumes are comparable, but the larger plasma and first-wall surface area of the SPPS/MHH results in a lower neutron wall load, as seen below in the comparison of engineering parameters. Energy confinement is similar in the two conceptual designs. In both cases, the radiation fraction, $f_{RAD} \simeq 0.2$, helps to spread the surface heat flux over the entire first wall and relieve the heat flux on the divertor plates.

3.3.2. Engineering

Engineering parameters of the SPPS/MHH and ARIES-II are summarized comparatively in Table 3.3-II. The SPPS/MHH is constrained to operate at a somewhat lower peak magnetic field strength as a concession to the uncertainties introduced by its non-planar coil technology. Should this concern be dissipated by future experience, the MHH design could be improved by access to higher fields and correspondingly higher power

Table 3.3-I.
Physics Parameters

	ARIES-II	SPPS/MHH
Plasma major toroidal radius, R_T (m)	5.60	13.95
Plasma minor radius, a_p (m)	1.40	1.16
Plasma vertical elongation, $\kappa_\times$	2.03	2.00
Plasma vertical elongation, κ_{95}	1.80	(1.77)
Plasma triangularity, $\delta_\times$	0.67	NA
Plasma triangularity, δ_{95}	0.48	NA
Plasma volume, V_p (m^3)	399	735
Plasma aspect ratio, $A = R_T/a_p$	4.0	12.08
Plasma aspect ratio, $A^\star = R_T/r_p$	NA	8.54
Circularized safety factor, q_*	4.6	NA
Plasma-edge safety factor, q	12.2	NA
Troyon coefficient, C_T (Tm/MA)	0.059	NA
Plasma beta, β	0.034	0.050
Plasma poloidal beta, β_θ	5.40	NA
Stability parameter, $\epsilon\beta_\theta$	1.35	NA
Ion temperature, T_i (keV)	10.0	10.0
Electron temperature, T_e (keV)	10.3	10.5
Ion density, n_i (10^{20} m^{-3})	2.15	1.31
Electron density, n_e (10^{20} m^{-3})	2.50	1.46
Particle-to-energy confinement time ratio, τ_p/τ_E	9.80	4.00
Ion-to-electron energy confinement time ratio, τ_{Ei}/τ_{Ee}	1.0	1.0
Lawson parameter, $n_i\tau_E$ (10^{20}s/m^3)	2.71	2.55
ITER-89P scaling [63] multiplier, H	3.07	NA
Lackner-Gottardi [10, 11] multiplier, H	NA	2.3
On-axis toroidal field, B_o (T)	7.97	4.94
Radiation fraction, f_{RAD}	0.18	0.21
Plasma current, I_ϕ (MA)	6.43	∼0
Bootstrap-current fraction, f_{BC}	0.87	∼0
Current-drive power to plasma, P_{CD} (MW)	66.1	0.0
Current-drive efficiencies:		
I_p/P_{CD} (mA/W)	13.06	NA
γ(10^{20} A/W-m^2)	0.18	NA

Table 3.3-II.
Engineering Parameters

	ARIES-II	SPPS/MHH
Field at TF coil, B_c(T)	15.9	14.5
TF-coil stress (MPa)	633	TBD
TF-coil current density (MA/m^2)	31.6	30.0
Stored magnetic energy (GJ)	83[a]	80 (est.)
Fusion power, P_F (GW)	1.91	1.73
Neutron power, P_N (GW)	1.53	1.38
Average neutron wall load, I_w (MW/m^2)	2.90	1.18
Peak neutron wall load, $\hat{I}_w$ (MW/m^2)	5.08	2.11
Neutron fluence life, $I_w\tau$ (MW yr/m^2)	16.4	16.4
Average blanket energy multiplication	1.38	1.40
Average first-wall heat flux, q_w(MW/m^2)	0.31	0.29
Blanket power density, P_{TH}/V_{BLK} (MW/m^3)	10.7	6.03
Current-drive system efficiency, η_{CD}	0.54	NA
Thermal conversion efficiency, η_{TH}	0.46	0.46
Thermal power, P_{TH}(GWth)	2.57	2.29
Auxiliary site power, P_{AUX} (MW)	47.3	42.2
Primary loop pumping power (MW)	11.8	10.5
Gross electrical power, P_{ET}(GWe)	1.18	1.05
Net electrical power, P_E(GWe)	1.0	1.0
Recirculating power fraction, $\epsilon = 1/Q_E$	0.15	0.052
Plasma gain, $Q_p = P_F/P_{CD}$	28.9	~2000
Engineering gain, Q_E	6.49	19.28
Net plant efficiency, $\eta_p = \eta_{TH}(1-\epsilon)$	0.39	0.44
Plant capacity factor, p_f	0.76	0.76
Masses (ktonne):		
First wall, blanket, and reflector	0.43	0.25
Shield	6.02	9.45
TF coils	1.81	4.10
PF coils	0.59	NA
Fusion power core	10.80	21.23
Mass power density, MPD (kWe/tonne)	92.6	47.1
Level of Safety Assurance, LSA	2	2

[a] TF: 65 GJ, PF: 18 GJ

density. As it stands, the average 14.1-MeV-neutron first-wall load is less than half that of the ARIES-II tokamak at the same net electrical power output, $P_E = 1.0$ GWe. With both devices invoking the self-cooled-Li/V blanket, the thermal conversion efficiency is taken to be $\eta_{TH} = 0.46$ in both cases. The Level of Safety Assurance (LSA) was set at 2 for both devices for purposes of cost credits. Absent the tokamak current-drive power requirement, the MHH has a significantly lower recirculating power fraction, ϵ. The cost benefit of the lower recirculating power offsets the implied penalty of lower power density on direct cost, as seen below.

3.3.3. Costing

For purposes of the projected Cost of Electricity (COE) calculation, both the ARIES-II and the SPPS/MHH are here taken to have the same (default) value of plant capacity factor, $p_f \simeq 0.76$. More detailed work in the area of reliability, availability, amd maintenance (RAM) anaylsis might well establish an advantage in this figure of merit for one of the two approaches. Differences in unscheduled (forced) outages based on the different configurations and loads are possible. Also, differences in scheduled downtime based on the details of the module changeout scenarios for the two devices can be postulated. Unfortunately, fixing the capacity factor partly decouples the COE projection from the design and obscures some dependancies which otherwise contribute to the identification of the 'near-optimum' design. Similarly, assuming the same construction lead time may tilt the comparative results somewhat. Both the ARIES-II and SPPS/MHH have been taken to have the same construction lead time, $\tau_c = 6$ yr, for purposes of calculating the time-related cost (*i.e.*, interest during construction). A more detailed consideration of both systems, with a view toward developing construction schedules, might be expected to generate some distinction resulting in a differential cost impact. The level of design work required to better establish some of the factors in the COE projection often is unavailable to the conceptual power-plant study. Such work was beyond the scope of the present SPPS, but should be addressed in any future work.

Comparative cost breakdowns for the ARIES-II and SPPS/MHH are summarized in Table 3.3-III, using 1992 as the reference year. Level of Safety Assurance (LSA) cost credits consistent with LSA = 2, reflecting a level of passive safety and lower source term (relative to fission), are assumed in both cases. COE values for LSA = 4 are also noted, consistent with full nuclear-safety-grade surcharges. The direct cost of the SPPS/MHH is found to be slightly higher than that of the ARIES-II which drives a higher total capital cost as well as a higher projected constant-dollar COE.

Table 3.3-III.
Economic Parameters (1992 $)

Acct. No.	Account Title	ARIES-II	MHH
		Million Dollars	
20.	Land and land rights	10.4	10.4
21.	Structures and site facilities	328.3	332.8
22.	Reactor plant equipment (RPE)	1361.8	1475.6
22.1.1	First wall, blanket, and reflector	53.8	71.5
22.1.2	Shield	366.4	289.8
22.1.3	Magnets	205.8	381.4
	TF coils	159.6	
	PF coils	46.2	
22.1.4	Supplemental heating systems	194.3	54.2
22.1.5	Primary structure and support	35.3	149.7
22.1.6	Reactor vacuum systems	51.1	85.4
22.1.7	Power supplies	55.3	55.3
22.1.8	Impurity control	5.4	12.0
22.1.9	Direct energy conversion system	NA	NA
22.1.10	ECRH breakdown system	4.3	4.3
22.1	Reactor equipment (RE)	971.7	1103.6
22.2	Main heat transfer and transport	231.9	217.8
23.	Turbine plant equipment (TPE)	279.8	254.0
24.	Electric plant equipment (EPE)	109.5	103.6
25.	Miscellaneous plant equipment (MPE)	55.5	51.9
26.	Special materials	14.8	21.0
90.	Total direct cost	2160.3	2249.4
91.	Construction services and equipment	259.2	269.9
92.	Home office engineering and services	112.3	117.0
93.	Field office engineering and services	129.6	135.0
94.	Owner's costs	399.2	415.7
96.	Project contingency	516.5	537.8
97.	Interest during construction (IDC)	590.9	615.3
98.	Escalation during construction (EDC)	0.	0.
99.	Total capital cost	4168.3	4340.2
		Constant dollars	
[90]	Unit direct cost, UDC ($/kWe)	2,160.4	2,249.4
[94]	Unit base cost, UBC ($/kWe)	3,577.4	3,724.8
[99]	Unit total cost, UTC ($/kWe)	4,168.4	4,340.2
	Capital return (mill/kWeh)	60.52	63.02
[40-47,51]	O&M (mill/kWeh)	9.16	9.16
[50]	Blanket replacement (mill/kWeh)	3.63	1.90
	Decommissioning (mill/kWeh)	0.50	0.50
[02]	Fuel (mill/kWeh)	0.03	0.03
	Cost of electricity, COE (mill/kWeh)[a]	73.84	74.60

[a] LSA = 2; values are 84.06 and 85.39, respectively, for LSA = 4.

At ~74 mill/kWeh, it would not be possible to discriminate between the two approaches on the basis of cost in light of the conceptual nature of the supporting studies for each and the many remaining uncertainties. Improvements in both approaches leading to lower COE values are recognized as being desireable, but difficult to achieve, given the fundamental constraints presently understood for magnetic fusion. The ratios of reactor equipment (RE) to reactor plant equipment (RPE) direct costs are $RE/RPE = 0.71$ and 0.75 for the ARIES-II and SPPS/MHH, respectively. The ratios of RPE direct cost to the total direct cost (TDC) are $RPE/TDC = 0.63$ and 0.66, respectively. The ratios of TDC to total capital cost (TCC) are 0.52 in both cases, given the common financial factors and (assumed) common construction time. The tabulated data regarding these cost components are summarized comparatively in Fig. 3.3-1 as histograms to facilitate the comparison between ARIES-II and the SPPS/MHH, and to highlight the cost drivers.

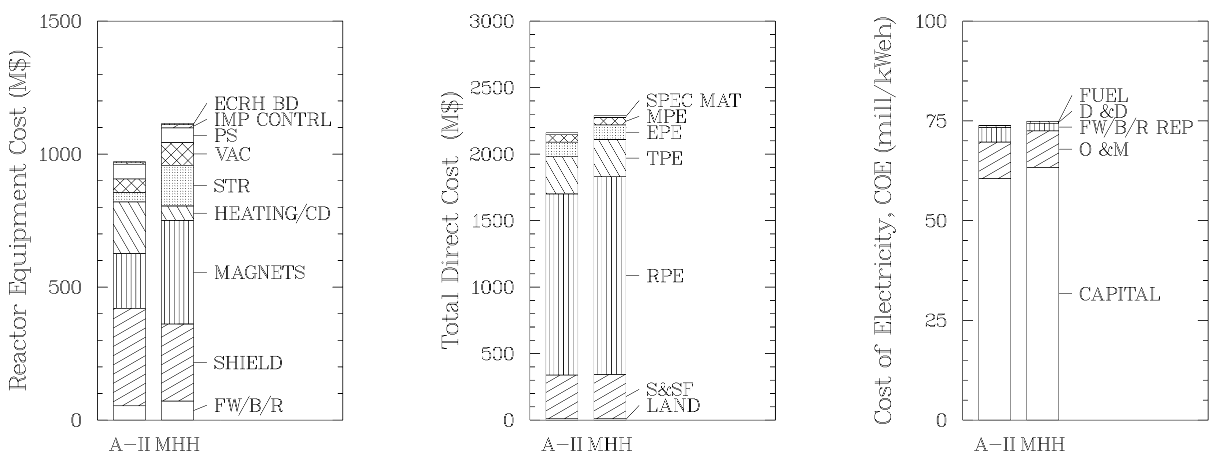

Figure 3.3-1. Cost breakdown of the reactor equipment cost (left), the direct cost (middle), and the cost of electricity (right) in 1992 $ for the ARIES-II tokamak and the SPPS/MHH power plants. The abbreviations used are: FW/B/R for first wall, blanket, and reflector; HEATING for supplemental-heating and current-drive systems; STR for primary structure and support; VAC for vacuum systems; PS for power supply, switching and energy storage; IMP CONTRL for impurity control; ECRH BD for ecrh breakdown system; S&SF for structures and site facilities; RPE, TPE, EPE, and MPE for reactor, turbine, electric, and miscellaneous plant equipment, respectively; SM for special materials; CAPITAL for capital return; O&M for operations and maintenance; REPLACE for FW/B/R replacement; and D&D for decontamination and decommissioning.

Having created a comprehensive, albeit simplified, model integrating physics, engineering, and cost considerations, it is hardly avoidable that it be exercised to determine the 'near-optimal' SPPS/MHH configuration, subject to the set of constraints and assumptions described here. Some notice should also be taken of the unquantified considerations (*e.g.*, complexity, technology extrapolation, and risk) that are also key aspects of the characterization of a viable, competitive future energy source. These considerations are not generally tractable in such studies as the SPPS.

3.4. PARAMETRICS AND SENSITIVITIES

To establish the context for the reference SPPS/MHH reference design described in the previous subsection, a number of parametric and sensitivity scans using the ASC* were performed. Both physics and engineering parameters were addressed with a view toward identifying any high-leverage factors deserving attention in follow-on power-plant studies or emphasis in the ongoing stellarator R&D effort.

To illustrate the impact of physics assumptions, Fig. 3.4-1 displays the impact of β on the projected COE. For this and subsequent figures, the plasma aspect ratio is fixed such that $A^\star \equiv R_T/r_p \simeq 8.54$. The major toroidal radius, R_T, is used as the independant search variable in the ASC*. As R_T increases, the FPC increases in size and direct cost, leading to higher COE values as system power density falls. For fixed net electrical output, P_E, and fixed thermal conversion efficiency, η_{TH}, the product $(\beta^2 B^4 V_p)$ is a constant, with larger, lower-power-density devices allowing for lower magnetic-field strengths at both the plasma axis and at the modular coil windings, as monitored by B_c (T). The apparent incentive is to reduce the size of the FPC while maximizing the value of B_c up to any imposed technology limit. Choice of the limiting peak coil field strength, $B_c \simeq 14.5\,T$, precludes access to smaller, cheaper devices. Higher beta values than the 5% reference SPPS value, allow a more compact FPC with resultant cost reductions just as lower beta values lead to COE increases, as shown. With the plant capacity factor, p_f, held fixed, there is no higher-order availability/maintenance discriminator between devices of different size. Similarly, there is no higher-order discriminator deriving from different construction lead times, τ_c. A possibly important, but unknown, physics dependancy is that of the beta value on plasma aspect ratio, A. In the absence of information on this issue, a parametric search that proved to be salient in the ARIES tokamak studies could not be applied to the present SPPS work. The plasma temperature is fixed such that $T_i \simeq T_e \simeq 10$ keV, neglecting variations as plasma density, $n_{i,e}$, and confinement factor, H, adjust to the changing values of magentic-field strength, B, and V_p (m^3) to

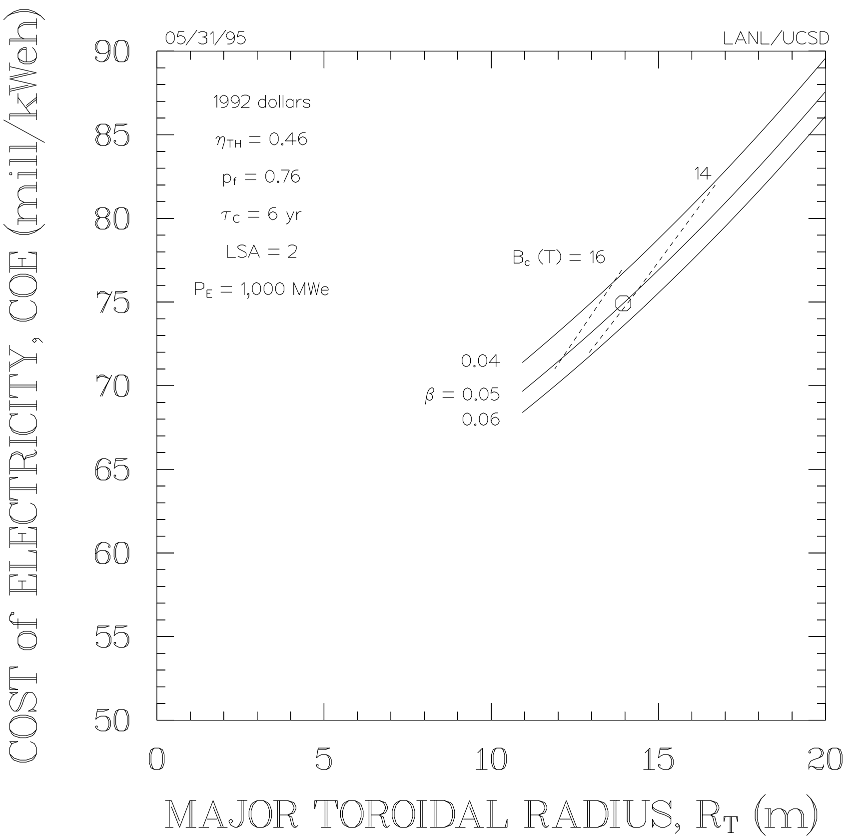

Figure 3.4-1. Dependence of MHH projected Cost of Electricity, COE, on effective major toroidal radius, R_T, for the indicated values of β and the indicated fixed parametes. Isoquants for several values of magnetic field strength at the coils, B_c, are indicated by the dashed lines. The reference SPPS/MHH design point with $\beta = 0.05$ is denoted by the open circle.

preserve the target net electrical power output, P_E (MWe). The reference SPPS/MHH design point is denoted explicitly.

Variations in the value of net electrical output power, P_E are shown in Fig. 3.4-2. The reference SPPS/MHH value is $P_E = 1,000\, MWe$, to facilitate certain direct comparisons with the ARIES and PULSAR tokamak designs. The economies of scale suggest lower projected COE values, for fixed plant capacity factor, $p_f \simeq 0.76$, as P_E increases. There is no fundamental inhibition standing in the way of matching the gross electrical output, $P_{ET}\,(MWe)$, MHH with the largest (single) turbogenerator unit available (currently $\sim 1,350\, MWe$ in the U.S. or $\sim 1,500\, MWe$ in France). The lower recirculating power of the stellarator, relative to the tokamak, allows the stellarator to take full advantage of

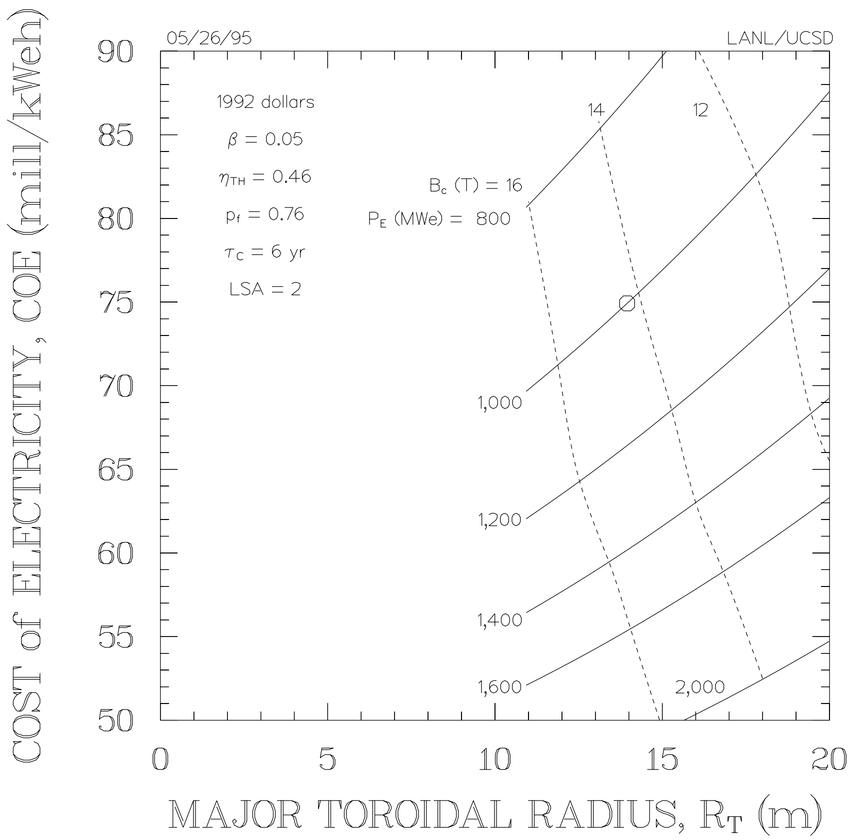

Figure 3.4-2. Dependence of projected MHH Cost of Electricity, COE, on effective major toroidal radius, R_T, for the indicated values of P_E and the indicated fixed parametes. Isoquants for several values of magnetic field strength at the coils, B_c, are indicated by the dashed lines. The reference SPPS/MHH design point with $P_E = 1,000$ MWe is denoted by the open circle.

the utilization of the largest available turbogenerator. Economies of large unit provide some incentive to develop even larger turbogenerators, but this approach stacks another development step in the path of fusion R&D. It is also possible to consider multiple turbogenerators of a nominal rating driven by a large FPC, but this approach incurrs some cost penalty and is not generally recommended. Absent the significant current drive recirculating power requirements of tokamak power plants, the typical stellarator plant could be deliberatly larger than a tokamak, with some cost benefit accruing to the stellarator. This issue has not been exploited in the course of the SPPS.

Additional consideration of the first-wall 14.1-MeV neutron wall load results in the dotted isoquants of Fig. 3.4-3 being added as an overlay to the results of Fig. 3.4-2. For the assumed fixed value of plant capacity factor, $p_f \simeq 0.76$, there is no direct influence of the (peak) wall load on the COE through the scheduled-componet-replacement contribution. Fixing the value of p_f represents a (default) starting assumption, pending further work. Degradation of the p_f at higher P_E will inhibit access to larger plants or a technological limit on surface heat flux or blanket power density will come into play as P_E increases.

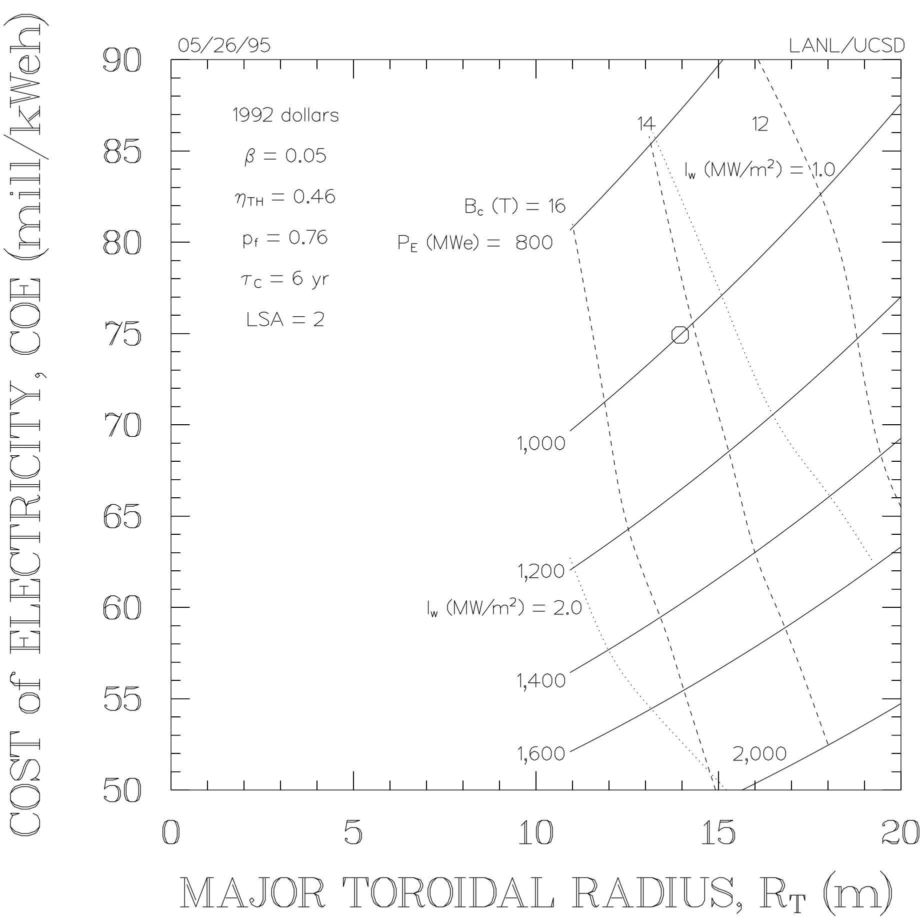

Figure 3.4-3. Dependence of MHH projected Cost of Electricity, COE, on effective major toroidal radius, R_T, for the indicated values of P_E and the indicated fixed parametes. Isoquants of average 14.1-MeV neutron first-wall load are shown. The reference MHH design point with $P_E = 1,000 MWe$ is denoted by the open circle.

Inclusion of a reliablility, availability, and maintenance (RAM) model, developed in the course of the PULSAR study [2], allows preliminary consideration of the adverse impact of higher first-wall neutron load (with fixed fluence lifetime) on the plant capacity factor, p_f. For each indicated value of net electrical power output, P_E, the COE projection is shifted upward, as seen in Fig. 3.4-4, as a result of the longer scheduled outage time to replace first-wall/blanket modules. This effect further inhibits consideration of larger plant sizes.

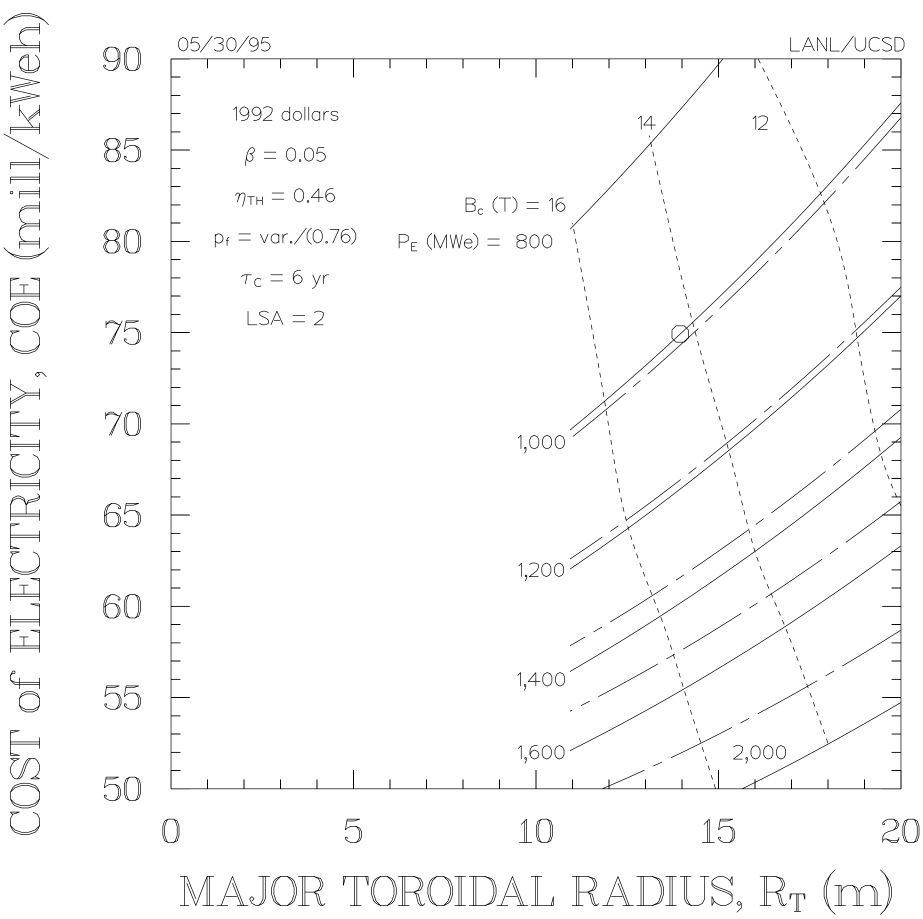

Figure 3.4-4. Dependence of MHH projected Cost of Electricity, COE, on effective major toroidal radius, R_T, for the indicated values of P_E and the indicated fixed parametes. The reference MHH design point is denoted by the open circle.

The reference SPPS/MHH coil technology assumes a Nb_3Sn superconductor. For larger FPCs at the same value of net electrical power output, P_E. the magnetic field will drop to the level at which NbTi superconductors, with lower unit costs, are appropriate. Such a transition does not result a design with costs near the reference SPPS/MHH design, as shown in Fig. 3.4-5, insofar as the cost differential between the conducter options is modest [1]. The homogenized coil cost simplification is only a preliminary convenience; a better treatment is recommended.

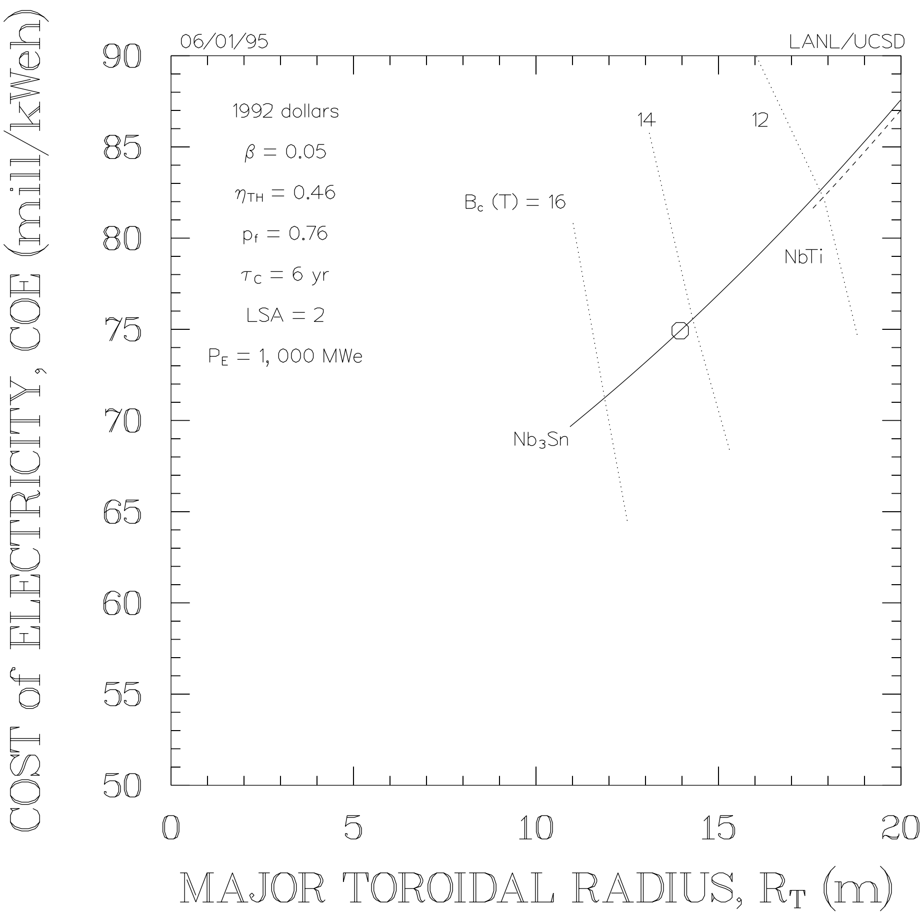

Figure 3.4-5. Dependence of MHH projected Cost of Electricity, COE, on effective major toroidal radius, R_T. The reference MHH design point is denoted by the open circle.

The economy of scale available to larger plant sizes is offset somewhat by the lower projected plant capacity factor, p_f, attributable to longer scheduled outages to replace first-wall/blanket sectors, as shown in Fig. 3.4-6. Here, an alternative parametric space is introduced to suggest that the plant capacity factor, p_f, and unit overnight cost, UOC (k\$/kWe), are independant drivers of the COE. To the extent that a compact FPC with low UOC is correlated with higher neutron wall load, the value of p_f should be reduced to track a larger scheduled maintenance downtime. Also, higher loads and stress can be expected to result in increased forced outages of the FPC, also resulting in lower values of p_f.

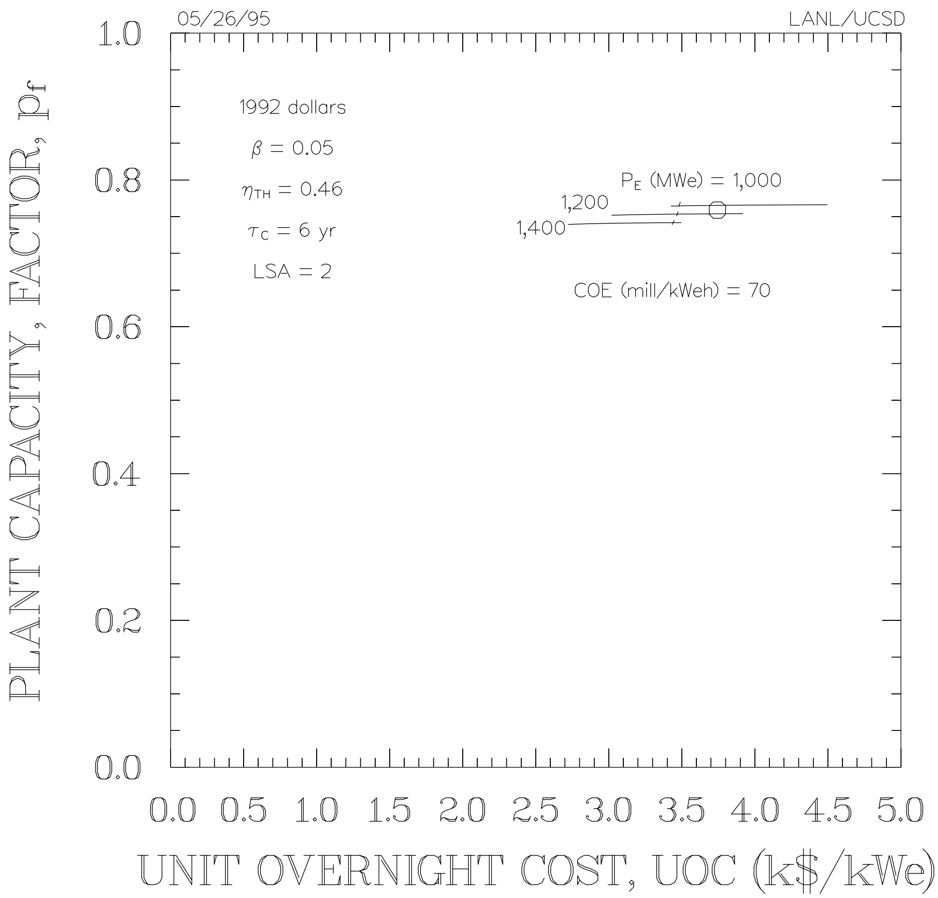

Figure 3.4-6. MHH phase space of plant capacity factor, p_f, and net electrical power output, P_E. An isoquant of $COE = 70\,mill/kWeh$ is indicated by the dashed line. The reference SPPS/MHH design point is denoted by the open circle.

The nominal SPPS/MHH construction lead time, τ_c was taken to be six years, in common with the ARIES and PULSAR studies. The coils and blanket/shield modules for all of these plants would be expected to be factory fabricated and shipped to the plant site and thus not constitute the critical path in the construction schedule. The larger FPC of the MHH results in a larger reactor hall than is required for the tokamaks, so it might be reasonable to consider a somewhat longer construction time. This relative penalty is considered a higher-order correction, beyond the scope of the present SPPS study, but is mentioned for consideration in future work. The corresponding COE penalty is a few mill/kWeh per year of "delay", as illustrated in Fig. 3.4-7. No additional dependence of the construction lead time on the major radius has been developed. A more detailed construction schedule, deriving from a more detailed power plant design effort, is required to resolve this issue.

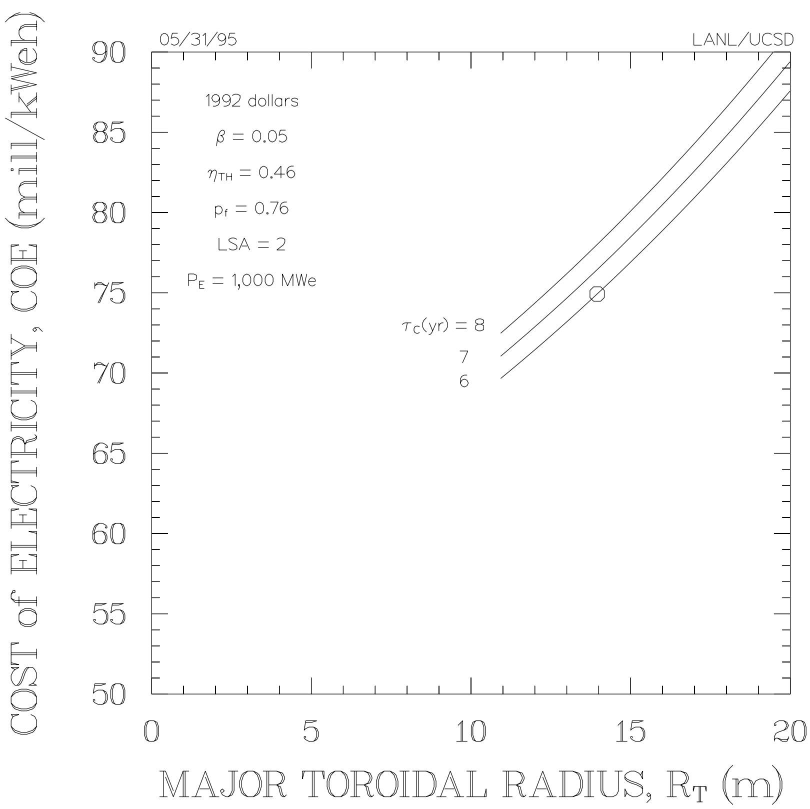

Figure 3.4-7. Dependence of MHH projected Cost of Electricity, COE, on effective major toroidal radius, R_T, for various values of costruction lead time, τ_c and the indicated fixed parameters. The reference SPPS/MHH design point, with $\tau_c = 6$ yr, is denoted by the open circle.

3.5. CONCLUSIONS

The systems analysis work performed in the course of the SPPS provides the basis for the conceptual design study by characterizing a plausible and integrated point design in terms of plasma physics, engineering, and economics. Several of the models used in the SPPS systems-code variant, ASC*, must be characterized as rudimentary and deserve refinement in any future work. While the design basis of the SPPS/MHH and the ARIES tokamak series is comparable, several aspects of the engineering have been improved in more recent versions of the tokamak ASC [65], as reflected in Starlite (Demo) candidates and the ARIES-RS (reversed shear) commercial power plant. It was not possible to back-fit these more recent considerations into the present SPPS/MHH description. Thus, the SPPS/MHH design is already somewhat out-of-step ('obsolete' is too harsh of a characterization). A strictly current reconciliation of evolving approaches to economics, as summarized in Refs. [29, 49], was similarly not back-fit to the SPPS/MHH.

Lacking certain scaling models, the SPPS/MHH design point should be considered representative, rather than an optimal configuration at the level of recent ARIES tokamak designs [64]. The 1,000-MWe class SPPS/MHH is seen to be reasonably competitive with tokamaks using the usual figures of merit. The low value of recirculating power helps to offset the disadvantages of fairly low power density. Some of the specialized attributes of the SPPS/MHH stellarator could well be exploited further to improve its competitive position. The stellarator could perhaps take advantage of economies of scale by positioning at a larger plant size than a tokamak, the latter being more constrained by surface-heat-load and power density considerations.

REFERENCES

[1] F. Najmabadi, R. W. Conn, *et al.*, "The ARIES-II and -IV Second-Stability Tokamak Fusion Power Plant Study—The Final Report," UCLA report UCLA-PPG-1461 (to be published); also, F. Najmabadi, R. W. Conn, *et al.*, "Directions for Attractive Tokamak Reactors: The ARIES-II and ARIES-IV Second-Stability Designs," *Proc. 14th Int. Conf. on Plasma Phys. and Controlled Nucl. Fusion Research,* Würzburg, Germany (Oct. 1992), International Atomic Energy Agency, Vienna (1993) 295.

[2] F. Najmabadi *et al.*, "The Pulsar Study– A Pulsed-Tokamak Fusion Power Plant," University of California, San Diego report UCSD-ENG-003 (1996).

[3] J. F. Lyon, K. Gulec, R. L. Miller, and L. El-Guebaly, "Status of the US Stellarator Reactor Study," *Fusion Eng. Des.,* **25** (1994) 85.

[4] J. A. Rome and S. P. Hirshman, "Curvilinear Formulae for Use with MHH," unpublished (March 30, 1994).

[5] F. Najmabadi, R. W. Conn, *et al.*, "The ARIES-I Tokamak Fusion Reactor Study—The Final Report," UCLA report UCLA-PPG-1323 (1991); also, R. W. Conn, F. Najmabadi, *et al.*, "ARIES-I: A Steady-State, First-Stability Tokamak Reactor with Enhanced Safety and Environmental Features," *Proc. 13th Int. Conf. on Plasma Phys. and Controlled Nucl. Fusion Research,* Washington, D.C. (Oct. 1990), International Atomic Energy Agency, Vienna (1991) 659.

[6] K. A. Werley, "Reversed Field Pinch Ignition Physics," Los Alamos National Laboratory document LA-UR-89-4093 (1989).

[7] K. A. Werley, "Reversed Field Pinch Ignition Requirements," *Nucl. Fusion,* **31** (1991) 576.

[8] H. S. Bosch and G. M. Hale, "Improved Formulas for Fusion Cross-Sections and Thermal Reactivities," *Nucl. Fusion,* **32** (1992) 611; also erratum *Nucl. Fusion,* **33** (1993) 1919.

[9] T. Kammash, "Fusion Reactor Physics: Principles and Technology," Ann Arbor Science Publishers, Inc., Ann Arbor (1975) 112.

[10] K. Lackner and N. A. O. Gottardi, "Tokamak Confinement in Relation to Plateau Scaling," *Nucl. Fusion,* **30** (1990) 767.

[11] A. Weller, *et al.,* "Optimum Confinement in the Wendelstein 7-AS Stellarator," *Plas. Phys. Cont. Fusion,* **33** (1991) 1559.

[12] U. Stroth, M. Murakami, R. A. Dory, H. Yamada, S. Okamura, F. Sano, and T. Obiki, "Energy Confinement Scaling from the International Stellarator Database", *Nucl. Fusion,* **36** (1996) 1063.

[13] J. R. McNally, Jr., "Physics of Fusion Fuel Cycles," *Nucl. Technol./Fusion,* **2** (1982) 9.

[14] M. Fujiwara, K. Yamazaki, M. Okamoto, J. Todoroki, T. Amano, *et al.,* "Large Helical Device (LHD) Program," *J. Fusion Energy,* **15** (1996).

[15] R. L. Miller, C. G. Bathke, R. A. Krakowski, F. M. Heck, L. Green, *et al.*, "The Modular Stellarator Reactor: A Fusion Power Plant," Los Alamos National Laboratory report LA-9737-MS (July 1983).

[16] H. M. Attaya and M. E. Sawan, "NEWLIT-A General Code for Neutron Wall Loading Distribution in Toroidal Reactors," *Fusion Technol.,* **8** (1985) 609.

[17] R. W. Conn (Chairman), "Panel X Report to the USDOE Magnetic Fusion Advisory Committee," University of California, Los Angeles document (May 1985).

[18] R. A. Krakowski, "Simplified Fusion Power-Plant Costing: A General Prognosis and Call for 'New Think'," *Fusion Technol.,* **27** (1995) 135.

[19] R. A. Krakowski, "Progress in Commercial Magnetic Fusion Energy Reactor Designs," *Fusion Technol.,* **20** (1991) 121.

[20] C. D. Beidler, G. Grieger, E. Harmeyer, J. Kiβlinger, N. Karulin, W. Mauer, J. Nührenberg, F. Rau, J. Sapper, and H. Wobig, "Helias Reactor Studies," Max-Planck-Institut für Plasmaphysik report IPP 2/330 (October 1995).

[21] R. W. Conn, J. P. Holdren, S. Sharafat, D. Steiner, D. A. Ehst, W. J. Hogan, R. A. Krakowski, R. L. Miller, F. Najmabadi, and K. R. Schultz, "Economic, Safety and Environmental Prospects of Fusion Reactors," *Nucl. Fusion,* **30** (1990) 1919.

[22] C. C. Baker, M. A. Abdou, R. M. Arons, A. E. Bolon, C. D. Boley, J. N. Brooks, *et al.*, "STARFIRE – A Commercial Tokamak Fusion Power Plant Study," Argonne National Laboratory report ANL/FPP-80-1 (September 1980).

[23] W. B. Hirschmann, "Profit from the Learning Curve," *Harvard Bus. Rev.,* **42** 1 (Jan-Feb 1964) 125.

[24] L. Argote and D. Epple, "Learning Curves in Manufacturing," *Science,* **247** (1990) 920.

[25] "Technical Basis for the ITER Interim Design Report, Cost Review and Safety Analysis," ITER EDA Documentation Series No. 7, International Atomic Energy Agency, Vienna (1996).

[26] S. L. Thomson, "Cost Algorithms for Superconducting Magnets," Oak Ridge National Laboratory document FEDC-M-88-ITER-001 (October 1988).

[27] J. G. Delene and C. R. Hudson II, "Cost Estimate Guidelines for Advanced Nuclear Power Technologies," Oak Ridge National Laboratory report ORNL/TM-10071/R3 (May 1993).

[28] J. G. Delene, K. A. Williams, and B. H. Shapiro, "Nuclear Energy Cost Data Base," US DOE report DOE/NE-0095 (September 1988).

[29] T. C. Hender, P. J. Knight, and I. Cook, "Key Issues for the Economic Viability of Magentic Fusion Power," *Proc. of ANS 12th Top. Mtg. Technol. of Fusion Energy,* Reno, NV, (June 1996), *Fusion Technol.* **30** (1996) 1605.

[30] B. Badger, I. N. Sviatoslavsky, S. W. Van Sciver, G. L. Kulcinski, G. A. Emmert, D. T. Anderson, *et al.*, "UWTOR-M: A Conceptual Modular Stellarator Power Reactor," University of Wisconsin report UWFDM-550 (October 1982).

[31] R. A. Krakowski, R. L. Hagenson, N. M. Schnurr, C. Copenhaver, C. G. Bathke, and R. L. Miller, "Compact Reversed-Field Pinch Reactors (CRFPR)," *Nucl. Eng. Des./Fusion,* **4** (1986) 75.

[32] B. G. Logan, C. D. Henning, G. A. Carlson, R. W. Werner, D. E. Baldwin, W. L. Barr, *et al.*, "MARS Mirror Advanced Reactor Study Final Report," Lawrence Livermore National Laboratory report UCRL-53480 (July 1984).

[33] F. Najmabadi, R. W. Conn, R. A. Krakowski, K. R. Schultz, D. Steiner, and the TITAN Research Group, "The TITAN Reversed-Field-Pinch Reactor Study—The Final Report," University of California Los Angeles, General Atomics, Los Alamos National Laboratory, and Rensselaer Polytechnic Institute, University of California Los Angeles report UCLA-PPG-1200 (1990); also, F. Najmabadi, R. W. Conn,

R. A. Krakowski, K. R. Schultz, D. Steiner, and the TITAN Research Group, "Engineering and Physics of High-Power-Density, Compact, Reversed-Field-Pinch Fusion Reactors: The TITAN Study," *Proc. 15th Symp. Fusion Technol. (SOFT),* Utrecht, the Netherlands (Sept. 1988), *Fusion Technology 88*, A. M. Van Ingen, A. Nijsen-Vis, H. T. Klippel, Eds., North-Holland, Amsterdam (1989) 1779.

[34] F. Najmabadi, R. W. Conn, *et al.*, "The ARIES-III D-^{3}He Tokamak Reactor Study–The Final Report," UCLA report UCLA-PPG-1323 (to be published); also, F. Najmabadi, R. W. Conn, *et al.*, "The ARIES-III D-^{3}He Tokamak Reactor Study," *Proc. IEEE 14th Symp. on Fusion Eng.,* San Diego, CA (Oct. 1991), IEEE No. 91CH3035-3, IEEE, Piscataway, NJ (1992) 213.

[35] J. G. Delene, "GENEROMAK Cost Model Update," Oak Ridge National Laboratory, private communication (February 1989).

[36] R. L. Miller, "Fusion Reactor Cost Reality Check," Los Alamos National Laboratory memorandum A-3:93-252(U) (August 13, 1993).

[37] H. Bruschi and T. Andersen, "Turning the Key," *Nucl. Eng. Intl.,* **36** (1991) 15.

[38] J. D. Mottley, "Electricity Generation Cost Reduction with the AP600 Reactor," *Trans. Amer. Nucl. Soc.,* **69** (1993) 340.

[39] T. U. Marston, W. H. Layman, and G. Bockhold, Jr., "Utility Requirements for Safety in the Passive Advanced Light-Water Reactor," *Nucl. Safety,* **34** (1993) 84.

[40] J. D. Stevenson, "Designing for Extreme Loads-the Impact on Cost and Schedule," *Nuclear Engineering International,* **29** (1984) 30.

[41] S. J. Piet, "Approaches to Achieving Inherently Safe Fusion Power Plants," *Fusion Technol.,* **10** (July 1986) 7.

[42] J. P. Holdren, D. H. Berwald, R. J. Budnitz, J. G. Crocker, J. G. Delene, R. D. Endicott, M. S. Kazimi, R. A. Krakowski, B. G. Logan, and K. R. Schultz, "Report of the Senior Committee on Environmental, Safety, and Economic Aspects of Magnetic Fusion Energy," Lawrence Livermore National Laboratory report UCRL-53766 (1989); also, J. P. Holdren, D. H. Berwald, R. J. Budnitz, J. G. Crocker, J. G. Delene, R. D. Endicott, M. S. Kazimi, R. A. Krakowski, B. G. Logan, and K. R. Schultz, "Exploring the Competitive Potential of Magnetic Fusion Energy: The Interaction of Economics with Safety and Environmental Characteristics," *Fusion Technol.* **13** (1988) 7.

[43] J. G. Delene, "LSA Cost Factors for Fusion Reactors," Oak Ridge National Laboratory, private communication (December 1990).

[44] I. Maya, K. R. Schultz, R. F. Bourque, E. T. Cheng, R. L. Creedon, J. H. Norman, *et al.*, "Inertial Confinement Fusion Reaction Chamber and Power Conversion System Study," General Atomics report GA-A17842 (October 1985).

[45] J. D. Lee, Ed., "MINIMARS Conceptual Design: Final Report," Lawrence Livermore National Laboratory report UCID-20773 (1986).

[46] J. G. Delene, R. A. Krakowski, J. Sheffield, and R. A. Dory, "GENEROMAK Fusion Physics, Engineering, and Costing Model," Oak Ridge National Laboratory report ORNL/TM-10728 (June 1988).

[47] J. G. Delene, "Operation and Maintenance Cost Estimate for Fusion Power Plants," Oak Ridge National Laboratory, private communication (May 1990).

[48] J. G. Delene, "GENEROMAK Model Update," Oak Ridge National Laboratory, private communication (February 1989).

[49] R. L. Miller, "Fusion Power Plant Economics," *Fusion Technol., Proc. of ANS 12th Top. Mtg. Technol. of Fusion Energy,* Reno, NV, (June 1996), *Fusion Technol.* **30** (1996) 1599.

[50] U. S. Department of Energy, Office of Nuclear Energy, "Nuclear Energy Cost Data Base, A Reference Data Base for Nuclear and Coal-Fired Power Plant Power Generation Cost Analysis," USDOE report DOE/NE-0096 (September 1988).

[51] J. Sheffield, R. A. Dory, S. M. Cohn, J. G. Delene, L. Parsly, D. E. T. F. Ashby, and W. T. Reiersen, "Cost Assessment of a Generic Magnetic Fusion Reactor," *Fusion Technol.,* **9** (1986) 199.

[52] W. R. Hamilton, D. C. Keeton, and S. L. Thomson, "Cost Accounting System for Fusion Studies," Oak Ridge National Laboratory report ORNL/FEDC-85/7 (December 1985).

[53] S. C. Schulte, T. L. Wilke, and J. R. Young, "Fusion Reactor Design Studies–Standard Accounts for Cost Estimates," Battelle Pacific Northwest Laboratory report PNL-2648 (May 1978).

[54] D. L. Phung, "A Method for Estimating Escalation and Interest During Construction (EDC and IDC)," in *Proc. 2nd Miami Conf. on Alternative Energy Sources,* Miami, FL (December 1979).

[55] U. S. Atomic Energy Commission, "Power Plant Capital Costs- Current Trends and Sensitivity to Economic Parameters," USAEC report WASH-1345 (October 1974).

[56] J. G. Delene, "Updated Comparison of Economics of Fusion Reactors with Advanced Fission Reactors," *Fusion Technol.,* **19** (May 1991) 807.

[57] S. C. Schulte, W. E. Bickford, C. E. Willingham, S. K. Ghose, and M. G. Walker, "Fusion Reactor Design Studies - Standard Unit Costs and Cost Scaling Rules," Pacific Northwest Laboratory report PNL-2987 (September 1979).

[58] J. G. Delene, "Operation and Maintenance Cost Estimate for Fusion Power Plants," Oak Ridge National Laboratory, private communication (February 1989).

[59] L. Howles, "1992 Annual Review of Load Factors," *Nuclear Engineering International,* **38,** 465 (April 1993) 19.

[60] T. H. Lee, B. C. Ball, Jr., and R. D. Tabors, *Energy Aftermath,* Harvard Business School Press, Boston MA (1990).

[61] E. M. Blake, "U.S. Capacity Factors: Soaring to New Heights," *Nucl. News,* **36** (May 1993) 40.

[62] T. J. Dolan, "Fusion Power Economy of Scale," *Fusion Technol.,* **24** (1993) 97.

[63] D. E. Post, K. Borrass, J. D. Callen, S. A. Cohen, J. G. Cordey, F. Engelmann, *et al.,* "ITER Physics," International Thermonuclear Experimental Reactor documentation series No. 21 (November 1990).

[64] R. A. Krakowski, C. G. Bathke, R. L. Miller, and K. A. Werley, "Lessons Learned from the Tokamak Advanced Reactor Innovation and Evaluation Study (ARIES)," *Proc. of ANS 11th Top. Mtg. Technol. of Fusion Energy,* New Orleans, LA, (June 1994), *Fusion Technol.* **26** (1994) 1111.

[65] C. G. Bathke, "A Systems Assessment of the Five Starlite Tokamak Power Plants," *Proc. of ANS 12th Top. Mtg. Technol. of Fusion Energy,* Reno, NV, (June 1996), *Fusion Technol.* **30** (1996) 1637.